Stanford. Geothermal Program
Interdisciplinary Research
in Engineering and Earth Sciences
Stanford University
Stanford, California

A PHYSICAL MODEL OF A GEOTHERMAL SYSTEM --ITS DESIGN AND CONSTRUCTION AND ITS APPLICATION TO RESERVOIR ENGINEERING

by
Stephen Duane Chicoine

June 1975

This research was carried out
under Research Grant GI-34925
by the National Science Foundation

This report was prepared originally as a thesis submitted to the Department of Petroleum Engineering and the Committee on the Graduate Division of Stanford University in partial fulfillment of the requirements for the degree of Engineer.

ACKNOWLEDGEMENTS

I wish to acknowledge the willing assistance of my fellow students and members of the research project: Dr. Norio Arihara, Paul Atkinsan, and particularly, Hsiu-Kuo Chen.

In addition, I would like to thank my advisor, Dr. Henry J. Ramey, Jr., for his guidance throughout the study.

The research funding provided through National Science Foundation Grant GI-34925 is gratefully acknowledged. The Standard Oil Company of California was kind enough to support the cost of my graduate education through an Energy Studies Fellowship.

My thanks are also extended to Jon Grim, the project's technician and machinist, who expended a great deal of time and effort in lending me his expertise in the construction of the model.

I would like to include a special acknowledgement to Dr. Giancarlo E. Facca, an early pioneer in the field of geothermal energy, who imparted to me his drive and enthusiasm while under his employment prior to attending Stanford.

Most important, I wish to express my unlimited gratitude to my wife, Patty, whose constant patience and encouragement helped to pull me through the difficult periods.

TABLE OF CONTENTS

APPENDICES (cont.)

LIST OF FIGURES

LIST OF TABLES

PREFACE

The initial development of geothermal resources for electrical power generation was begun in 1904 at Larderello, Italy. However, it was to be over half a century before interest in geothermal resources in the United States became anything more than academic. Even recently, the development of The Geysers, the U. S.' lone operating field to date, was accomplished only through remarkable determination on the part of two men.

In the light of the sudden shock of the 1973 Arab oil embargo and the continuing threat of another such occurrence, public attention has finally become focused upon the potential of alternative energy sources. Present oil imports exceed 30% of the total U. S. consumption. But the public memory has historically been short, and to many uninformed citizens, the end of the emba-rgo signaled an end to the energy crisis. However, the development of new energy resources and technological advancement lag sharply behind demand--a demand which continues to climb at unprecedented rates.

The road to total energy independence involves the utilization of all possible resources. And certainly, the advantages offered by geothermal energy are clear. Relative to other energy sources, geothermal energy is clean and inexpensive. The direct utilization of geothermal resources for heating is an additional benefit, as is the ability of geothermal

power stations to be developed economically in small units. And a great deal of the technology is already available within the American petroleurn industry. This is exemplified by the present NSF-funded research program at Stanford University's Department of Petroleum Engineering on the study of the reservoir engineering of geothermal resources. Geothermal energy must be given a fair opportunity to aid the nation's growing energy needs.

STATEMENT OF TI-IE PROBLEM

In geothermal reservoirs wherein saturated steam and water coexist, water will be the wetting phase--relatively immobilized in small pores and crevices--and steam will be the non-wetting phase, filling the large pores within the system. As the system depletes, the decline in reservoir pressure results in a corresponding reduction in liquid saturation* as the liquid boils to form steam. In terms of two-phase flow, the permeability of the system to steam will increase while the permeability to liquid water will decrease. This should ultimately lead to a practical "irreducible liquid water saturation," commonly denoted by S_{wi}. This term, commonly used within the petroleum literature, refers to the point during desaturation of the porous medium where the decrease in the saturation of the wetting phase is extremely small for further large increases in capillary pressure. In a petroleum reservoir, this liquid would be non-recoverable by an immiscible displacement process (hence the term "irreducible"). However, in a geothermal system, continued pressure decline can lead to the boiling of the remaining "irreducible" liquid, and the possible formation of a superheated "dry"

*When the term "saturation" is used in this sense, it refers to the volumetric fraction of pore space occupied by the liquid. This should be distinguished from the context "saturation conditions" which refers to liquicl and gas in equilibrium in the thermodynamic sense, or "gas saturated," meaning a liquid saturated with dissolved gas.

steam reservoir. Boiling can best be understood by means of a vapor pressure curve.

The vapor pressure curve (Fig. 1) represents pressures and temperatures at which steam and water coexist in equilibrium (saturation conditions). The curve represents results for a planar liquid-vapor interface. Within porous media, interfaces would be expected to be curved. Interface curvature should cause a lowering of vapor pressure in a porous media. This effect would be most pronounced for the strongly curved interfaces expected at liquid saturations below the "irreducible" level. The practical result of capillary pressure effects, then, would be that the residual liquid's boiling temperature would be elevated for a given pressure.

It is the purpose of this study to investigate the importance of vapor pressure lowering phenomenon, and ascertain whether flat interface vapor pressure data[1,2,3] are appropriate for use in geothermal reservoir engineering. The physical model utilized in this study also affords the opportunity to investigate the general characteristics of the production of geothermal reservoirs on a small scale.

Fig. 1

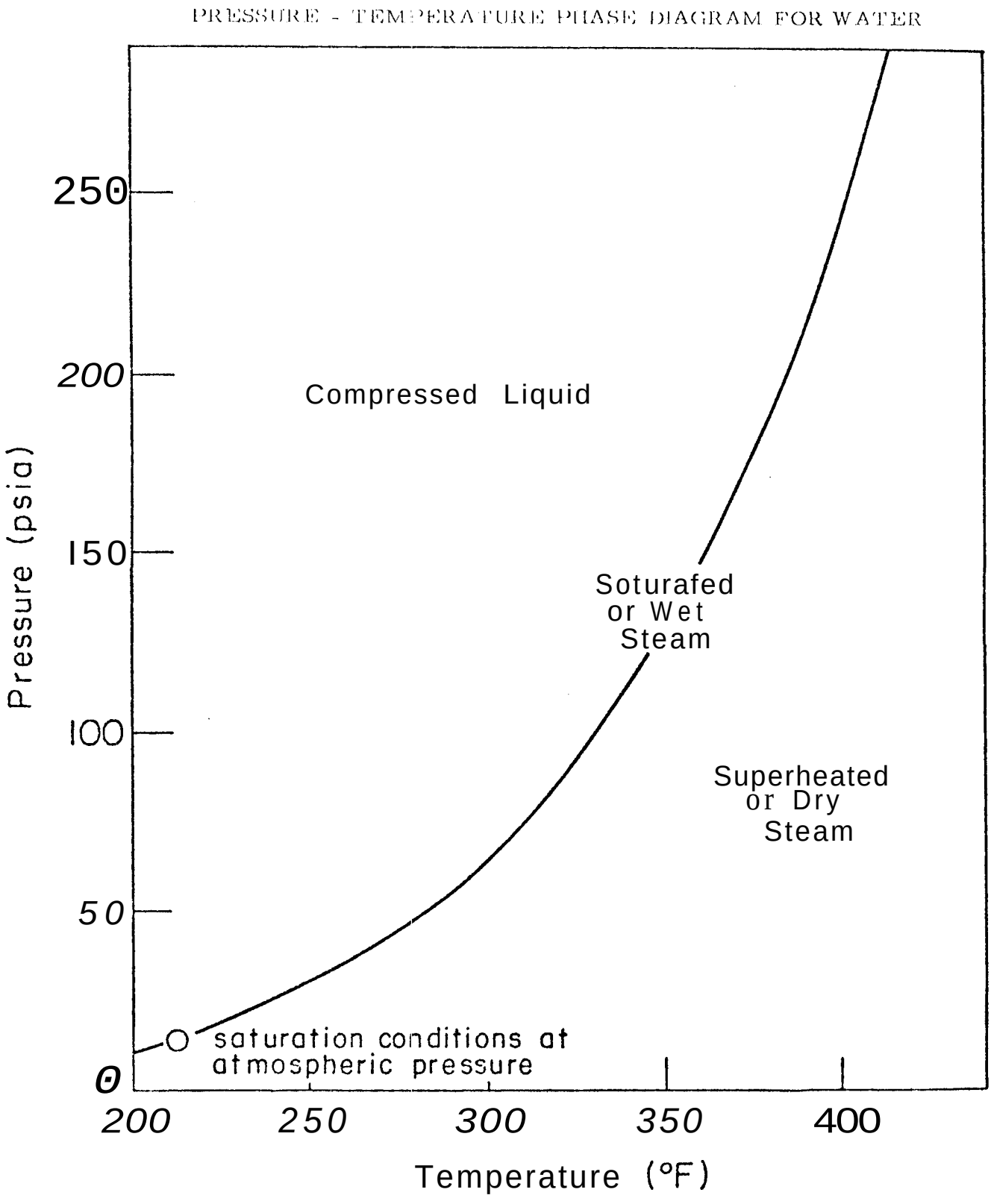
PRESSURE - TEMPERATURE PHASE DIAGRAM FOR WATER
Pressure (psia)
250
200
150
100
50
0
Compressed Liquid
Soturafed
or Wet
Steam
Superheated
or Dry
Steam
saturation conditions at
atmospheric pressure
200
250
300
350
400
Temperature (°F)

LITERATURE SURVEY

In a liquid-vapor system, boiling or vaporization occurs whenever the external absolute pressure imposed on the liquid is equal to or less than the vapor pressure of the liquid. Water can occur naturally within subsurface aquifers in the liquid state at temperatures far above the normal surface boiling temperature of 212^{o}E' due to the effect of pressure on boiling. Fig. 1, referred to earlier, illustrates the increase in vapor pressure with an increase in temperature relative to surface conditions. In order to understand geothermal reservoir behavior, it is critical to define the vapor pressure curve for conditions expected in geothermal reservoirs.

Consider a particular molecule of water at the liquid-vapor interface. The attraction toward the liquid is not compensated by an equal attraction from the more dispersed vapor molecules. Thus, it follows that the surface portions of the liquid have a higher free energy than the bulk liquid. This extra free energy is the surface or interfacial tension between the two fluids. As the laws of physical chemistry require that interfacial free energy be the minimum which is compatible with the volume of fluids present and the shapes of the restraining solid surfaces, the liquid surface always tends to contract to a minimum area. This is the basis of capillarity.[4]

In the 1800s, Lord Kelvin first deduced that, as a consequence of surface tension, the vapor pressure of a liquid is greater when in the form of a small droplet than when it has a planar surface.[5] In physical terms, there is less net attraction of the water molecules at the interface from the liquid droplet than in t'he case of a planar interface. This relationship is depicted in Fig. 2b. For the same reasons, the interfacial boundary is also curved when two immiscible fluids coexist in pore space.

But the liquid-vapor interface is concave toward the vapor phase. This curvature results in a greater net attraction by the liquid mass on the interfacial molecule relative: to the planar interface case (Fig. 2c). Consequently, a vapor pressure lowering phenomena is expected.

Conveyed in thermodynamic terms, any transfer of water molecules from the liquid to the vapor increases the area of the interface within the pore space and is, therefore, opposed by interfacial tension. This leads to increased stability of the liquid phase relative to the vapor phase in the pore space. This effect is expressed in a lower vapor pressure of the liquid. That is, for a given temperature, the absolute pressure must be lowered further before vaporization occurs. Or conversely, for a given pressure, the boiling temperature will be elevated (Fig. 3).

The curvature of an interface in static equilibrium gives rise to a pressure differential across the interface, which is known as the capillary pressure. The expression relating capillary pressure, p_c, to

Fig. 2 MOLECULAR ASPECTS OF VAPOR PRESSURE

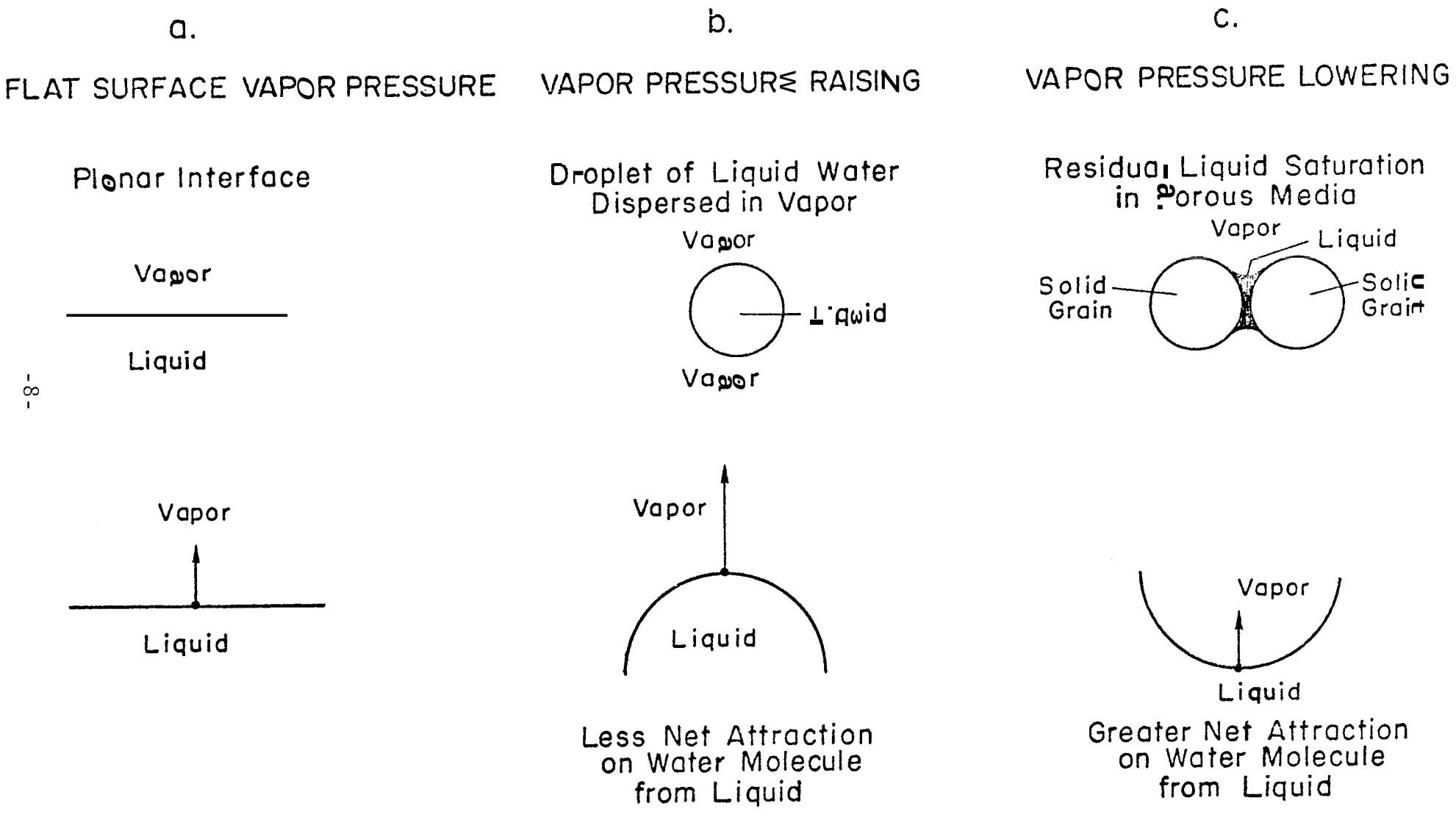

Fig. 3

BASIC EFFECT OF
INTERFACIAL TENSION
ON THE VAPOR PRESSURE CURVE
FOR WATER WITHIN POROUS MEDIA

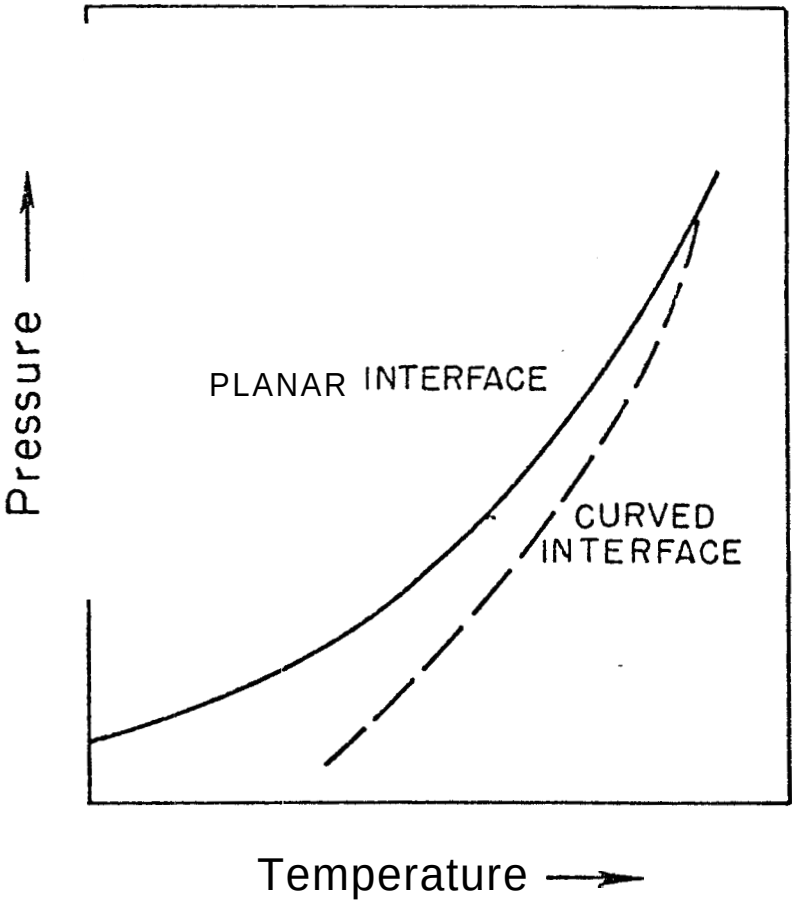

interfacial tension, σ, is the well-known LaPlace equation:[6]

$$p_c = \sigma (1/r_1 + 1/r_2) \qquad (1)$$

where r_1 and r_2 are the two principal radii of curvature at any point on the interface':

Leverett[4] noted that the degree of curvature of the interface between two fluids in a porous media depends upon the size of the intergranular spaces and the relative proportions of the fluids (that is, the liquid saturation). As both the vapor pressure above the curved interface and the capillary pressure across it are functions of the curvature of the surface, it can be concluded that both are also functions of the liquid saturation of the porous media. In fact, with extremely low liquid saturations and correspondingly strongly curved interfaces, capillary pressure effects within a porous media might result in a considerable degree of vapor pressure lowering. This is consistent with the relationships illustrated in Fig. 2.

A quantitative relationship between the vapor pressure above a curved interface, p_v, and the capillary pressure across it, p_c, in terms of measurable physical quantities can be developed by considering a porous

---

*The harmonic average of the two principle radii of curvature is the same at every point on the equilibrium interface. This is a mathematical consequence of the fact that the interfacial area is at a minimum. All methods of pore size determination that make use of capillary pressure are based on the claim t'hat the harmonic average of the principle radii of curvature of the interface can be related to the pore radius. 7

system containing water in equilibrium with its vapor (see Appendix A for complete derivation),, The simplified equation is shown below:

$$p_c = RT/M \quad \rho_l \quad \ln \; p_{vo}/p_v \qquad (2)$$

where

R is the ideal gas constant (10. 73 psi - ft^3)/(lb - mole - ^oR)
T is the ternperature (^{o} Rankine)
M is the molecular weight (lb/lb - mole)
ρ_l is the density of the liquid phase (lb/ft^3)
p_{vo} is the equilibrium vapor pressure above a flat interface between the liquid and its vapor (psi).

Calhoun, Lewis, and Newman[8] conducted a series of experiments designed to measure the lowering of the vapor pressure of water within a porous solid. Their experimental data from studies of synthetic consolidated core at 97^{o}F is shown. in Table 1. From the data, two important observations may be macle. First, there is an increased and significant lowering of the vapor pressure of water with decreased liquid saturation. Second, the effect appears to become more pronounced at the same level of liquid saturation in tighter sandstones (i.e., those of lower permeability). The data from Table 1 has been graphed on Fig. **4** to illustrate these two points. Whereas the experimental work of Calhoun, et al.,[8] was conducted at a temperature of 97^{o}F and is, therefore, not appropriate for the conditions encountered in geothermal reservoir systems; nonetheless, the presence of the phenomena within a porous media has been experimentally verified.

Ramey[9] indicated Calhoun[8] and co-workers had (apparently) mistakenly believed capillary pressure affected vapor pressure at liquid

Table 1

EXPERIMENTAL DATA
VAPOR PRESSURE LOWERING
AT 97°F

(Data from Calhoun, Ref. 8)

k = 3000 md, Ø = 0.321

S_w	p_{vo}/p_v	p_c*, cm of mercury
0. 0909	1.337	31,000
0. 0798	1. 782	61,900
0. 0676	2.941	116,000
0. 0570	3.922	147,000
0. 0496	5.917	191,000
0. 0487	9. 346	239,000
0. 0375	10. 526	252,000
0. 0319	24.096	340,000

k = 855 md, Ø = 0. 291

S_w	p_{vo}/p_v	p_c*, cm of mercury
0. 0962	1.052	5,430
0. 0744	3.289	127,000
0. 0668	4. 367	158,000
0. 0560	6.369	198,000
0. 0533	11.111	257,000
0. 0407	20.833	325,000

k = 760 md, Ø = 0. 279

S_w	p_{vo}/p_v	p_c*, cm of mercury
0. 103	1.101	10,250
0.079	3.344	129,000
0. 069	4. 796	168,000
0. 058	7.692	217,000
0. 0536	9. 709	243,000
0. 0479	19. 157	316,000
0. 0382	28.903	360,000
0.0325	37. 313	387,000

* p_c in cm of Hg (1 cm Hg = 0. 193 psi)

Fig. 4

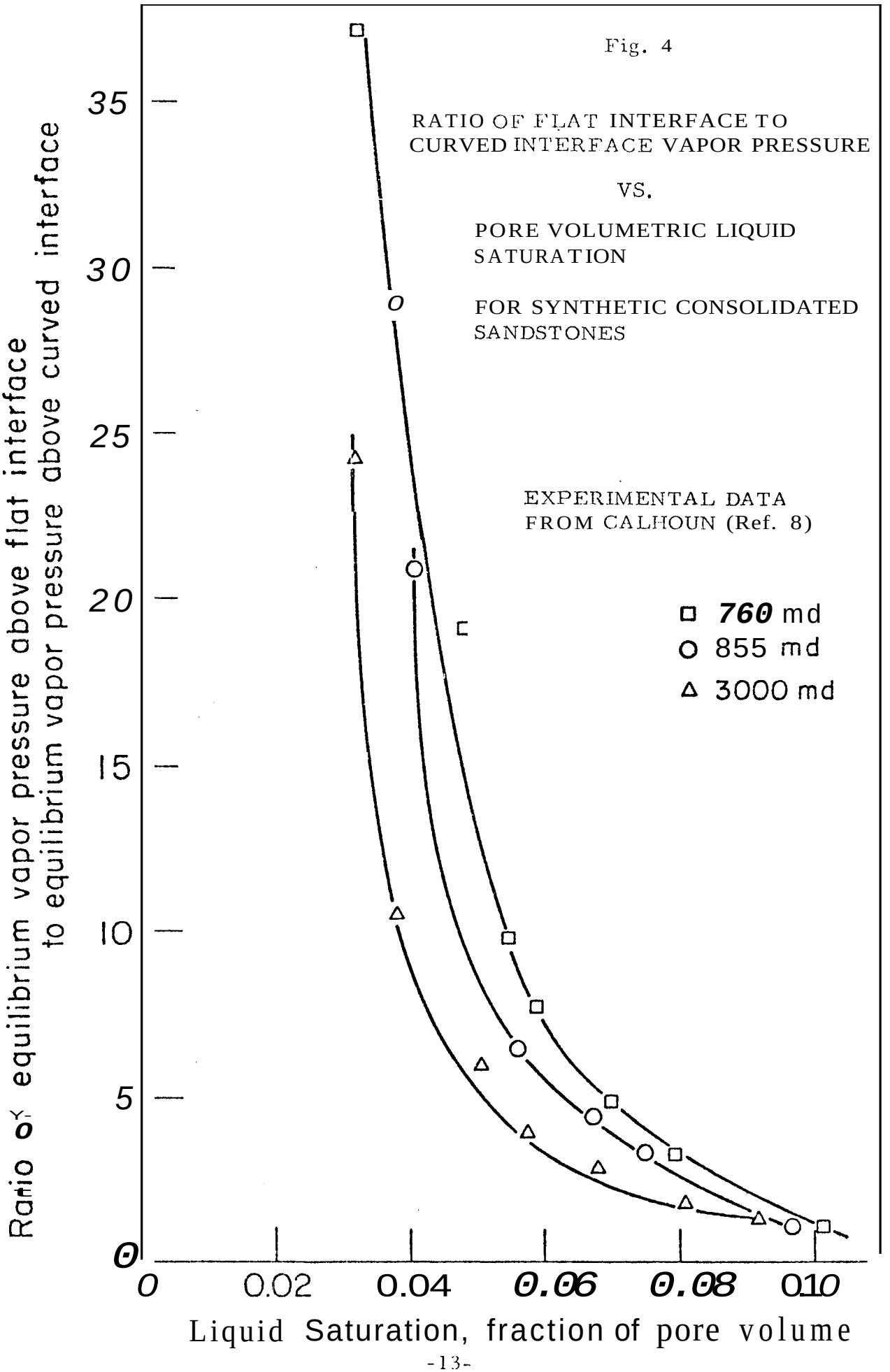
RATIO OF FLAT INTERFACE TO CURVED INTERFACE VAPOR PRESSURE
VS.
PORE VOLUMETRIC LIQUID SATURATION
FOR SYNTHETIC CONSOLIDATED SANDSTONES
EXPERIMENTAL DATA FROM CALHOUN (Ref. 8)
760 md
855 md
3000 md
Ratio of equilibrium vapor pressure above flat interface to equilibrium vapor pressure above curved interface
35
30
25
20
15
10
5
0
0
0.02
0.04
0.06
0.08
0.10
Liquid Saturation, fraction of pore volume

saturations greater than the practical irreducible level, S_{wi}. Instead, he felt that vapor pressure lowering would be evident only at liquid contents less than S_{wi} and would lead to a hysteresis effect below S_{wi}, as shown by Fig. 5. The figure, adapted from Cady,[10] was taken from this speculation by Ramey. 'The hysteresis would be caused by competing adsorption-desorption and the vapor pressure lowering. As the liquid film on the sand grains becomes thinner, the liquid-vapor interface of the film comes increasingly under the influence of the adsorptive forces of the solid surfaces. At exactly what liquid saturation or how important adsorption rnay be is not completely understood. It is generally assumed that the adsorptive field of a solid surface arises from unsatisfied electrostatic forces of the surface molecules.[11] As the electrostatic field surrounding a charged particle is not appreciably affected by temperature changes, Edlefsen and Anderson" hypothesized that the adsorptive field and its effects would not be altered to any great degree by variations in temperature.

Since interfacial tension between fluids is directly dependent upon intermolecular cohesive forces, its magnitude decreases with increasing temperature (the reader is referred to Fig. B1, Appendix B, for the qualitative relationship). Poston, et al.,[12] discovered that the irreducible water saturation for unconsolidated sands appeared to increase markedly with increasing temperature. This led to speculation that capillary pressure- liquid saturation curves were temperatures

Fig. 5

CAPILLARY PRESSURE AS A FUNCTION
OF LIQUID SATURATION IN POROUS MEDIA

(ADAPTED FROM CADY, Ref. 10)

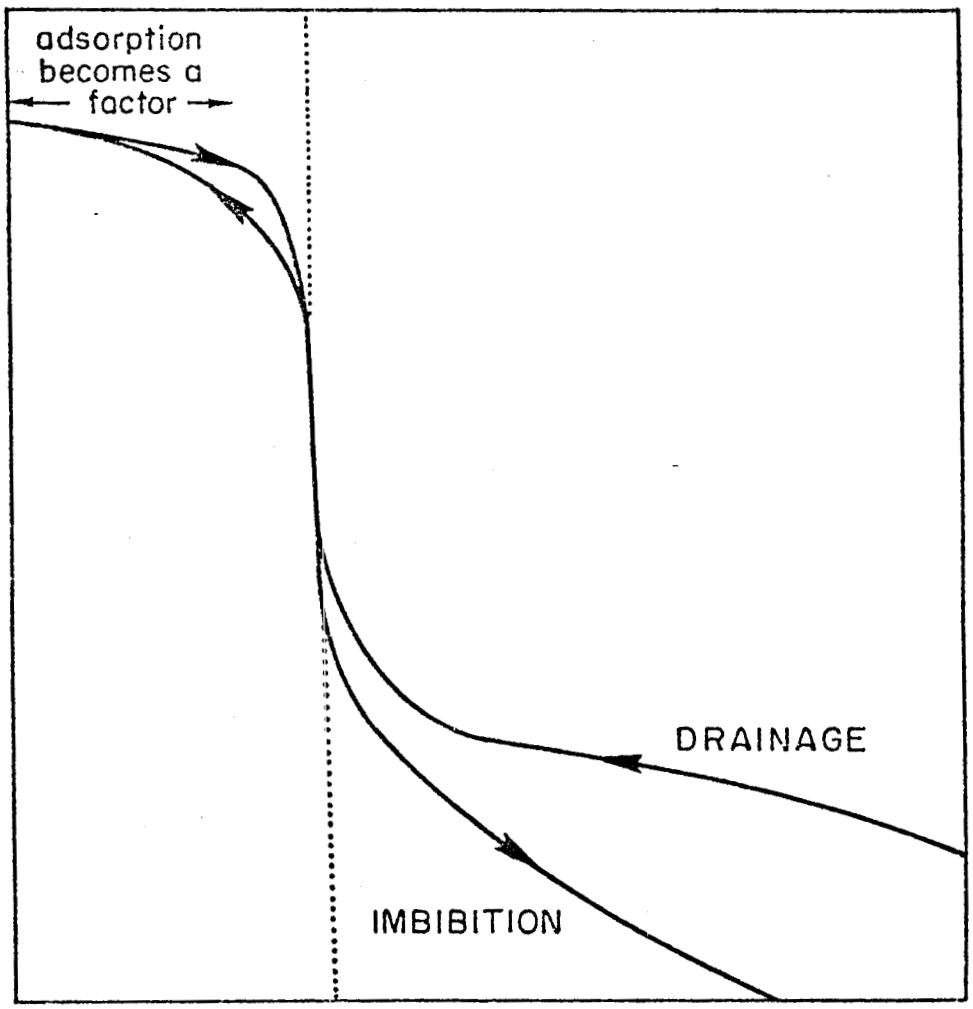

sensitive. Sinnokrot, et al.,[13] presented experimental evidence in support of this hypothesis as a result of studies with sandstone cores (only minor effects were observed for limestone cores). Hence, the phenomena of vapor pressure lowering due to capillary pressure effects is expected to be less significant at the temperatures commonly encountered in geothermal reservoirs.

It is important, therefore, to examine the expected magnitude of vapor pressure lowering at higher temperatures, on at least a theoretical basis. By combining eqs. 1 and 2, we obtain:

$$p_{vo}/p_v = \exp\left[(M\sigma/\rho_l RT)(1/r_1 + 1/r_2) \right] \qquad (3)$$

Unfortunately, straightforward calculations are not possible because of the r_1 and r_2 terms. In order to examine the magnitude of the phenomena, we need a range of values for the pore radii distribution, and we need to relate this set of values to the corresponding radii of curvature of the steam-liquid water interface. The alternative approach would be to begin with the Calhoun, et al.,[8] data and adjust the temperature-dependent variables (ρ_l, T, and σ). The results of the calculations for several temperature levels are shown in Fig. 6 (see Appendix B for a complete set of the calculations). Whereas the vapor pressure lowering effect is calculated to be considerably less at higher temperatures, the effect should still be evident in the 250°F - 350°F range. The major factor would appear to be the degree to which liquid saturation could be reduced.

Fig. 6

CALCULATED ISOTHERMS

FOR

RATIO OF FLAT INTERFACE TO CURVED INTERFACE VAPOR PRESSURE

VS.

PORE VOLUMETRIC LIQUID SATURATION

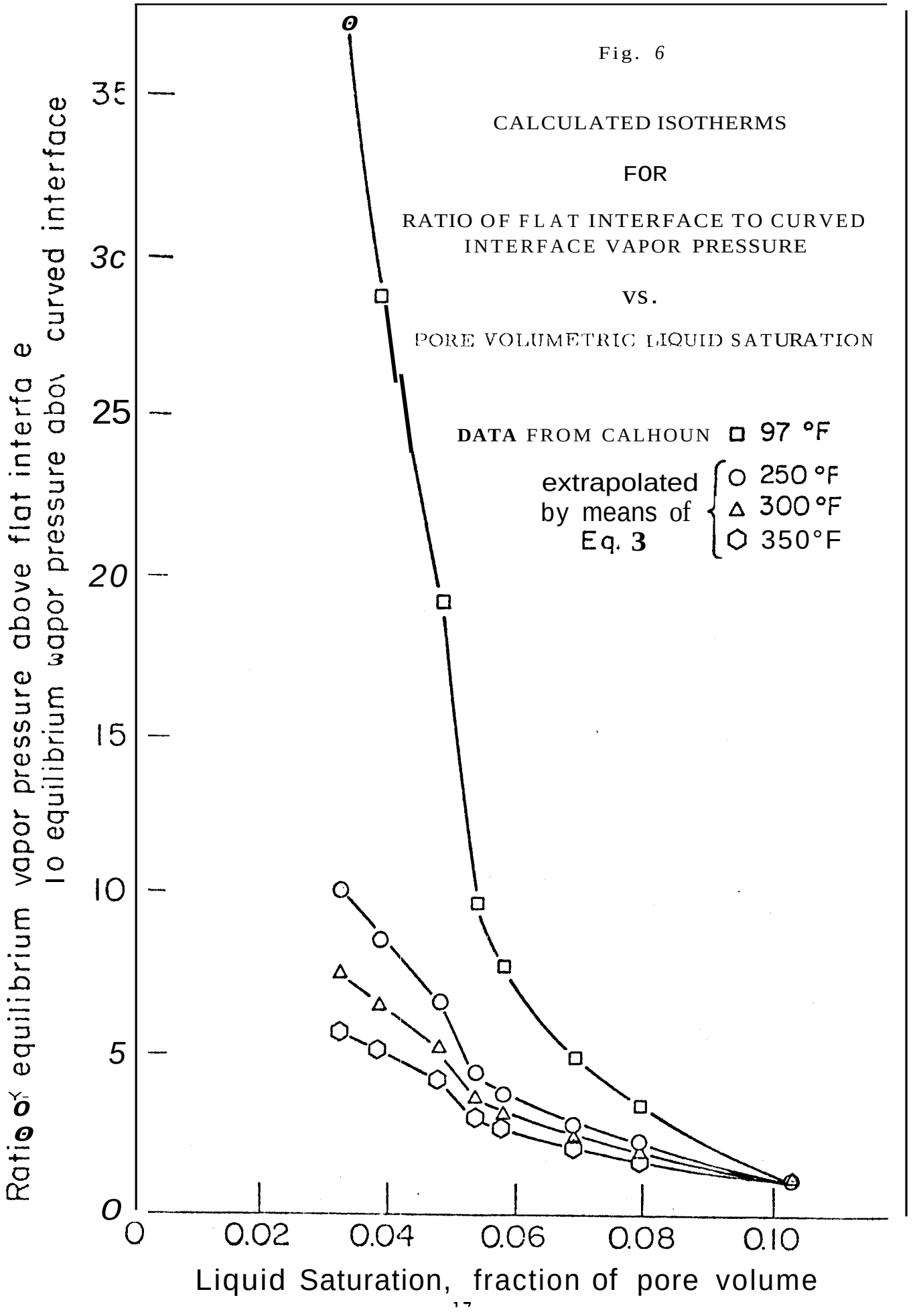

Cady's[10] doctoral dissertation was the first in a sequence of studies concerning model geothermal systems at Stanford. His results are shown on Fig. 7. On the basis of this data, Cady[10] concluded that vapor pressure lowering due to capillary pressure was not present in unconsolidated sands. Bilhartz'[14] work appeared to support this conctusion. It actually appeared that Cady[10] was able to vaporize all of the water in his sand pack. This is not surprising. Retention mechanisms depend largely on the process used to drain the porous media.[15] Whereas capillary retention (and the corresponding "irreducible" liquid saturation) becomes operative under the gravity drainage of a sand, vaporization should result in 100% recovery from the sand.

Whereas Calhoun's[8] work dealt with consolidated sandstones, both Cady[10] and Bilhartz[14] investigated unconsolidated sands. Capillary pressure phenomena are known to be quite different for consolidated and unconsolidated sands. Perhaps this could account for the contrast in results. Melrose and Brandner[16] observed that, in the case of a typical unconsolidated sand (closely sized particles), the wetting phase corresponding to the minimum saturation is largely in configurations known as pendular rings. That is, tho rings of liquid are wrapped around the contact point of two adjacent grains. As the particle size distribution widens, as in the case of a consolidated sand, the magnitude of the "irreducible" liquid Saturation increases. This additional fluid is trapped such that entire pores may he filled (funicular water). The contrasting capillary pressure drainage and imbibition curves for consolidated and unconsolidated sands are shown in Fig. 8.

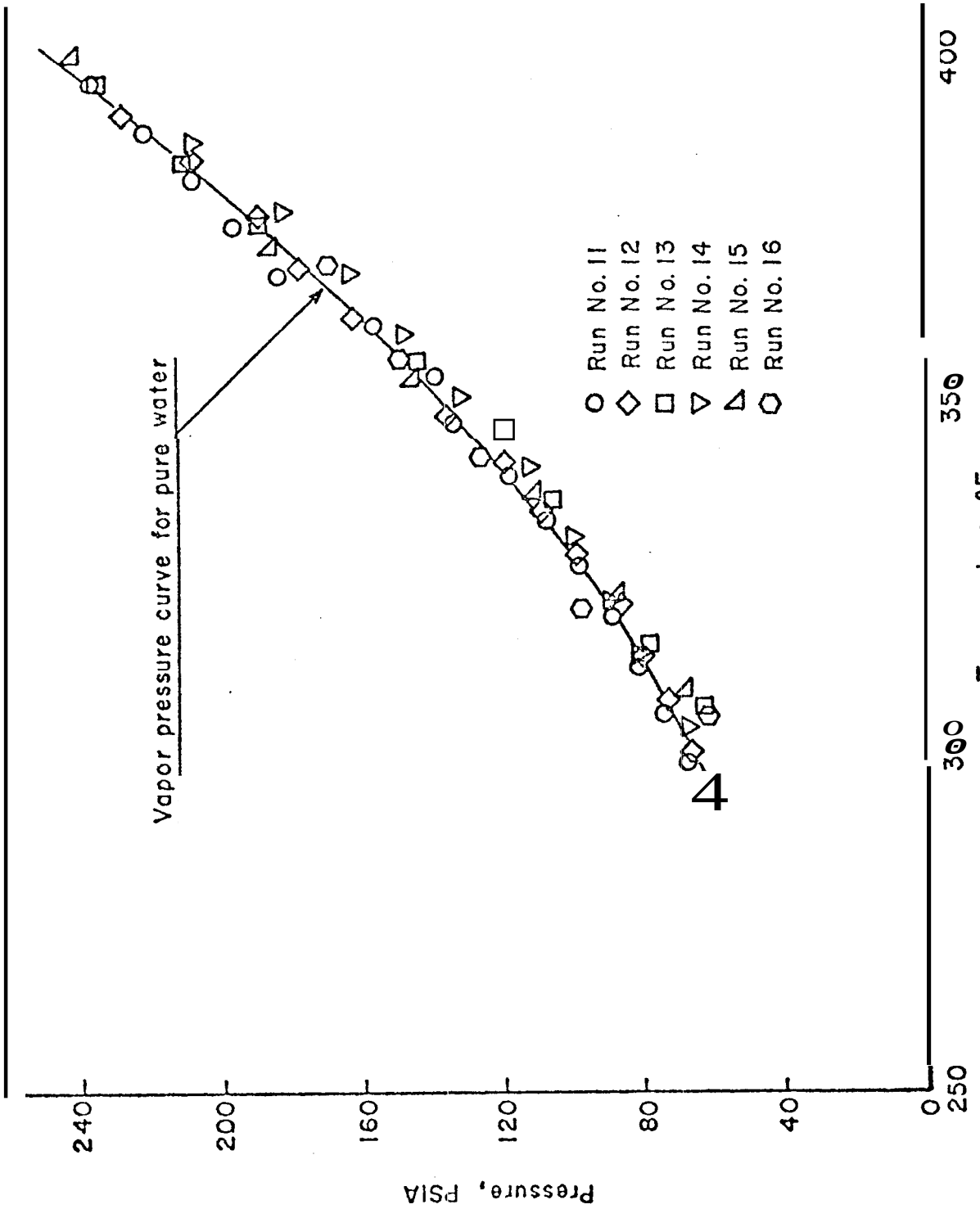

Fig. 7 Correlation of two-phase pressure and temperature during runs EXPERIMENTAL DATA FROM CADY (Ref. 10)

Fig. 8

CAPILLARY PRESSURE VS. WETTING PHASE SATURATION
FOR
CONSOLIDATED AND UNCONSOLIDATED SANDS

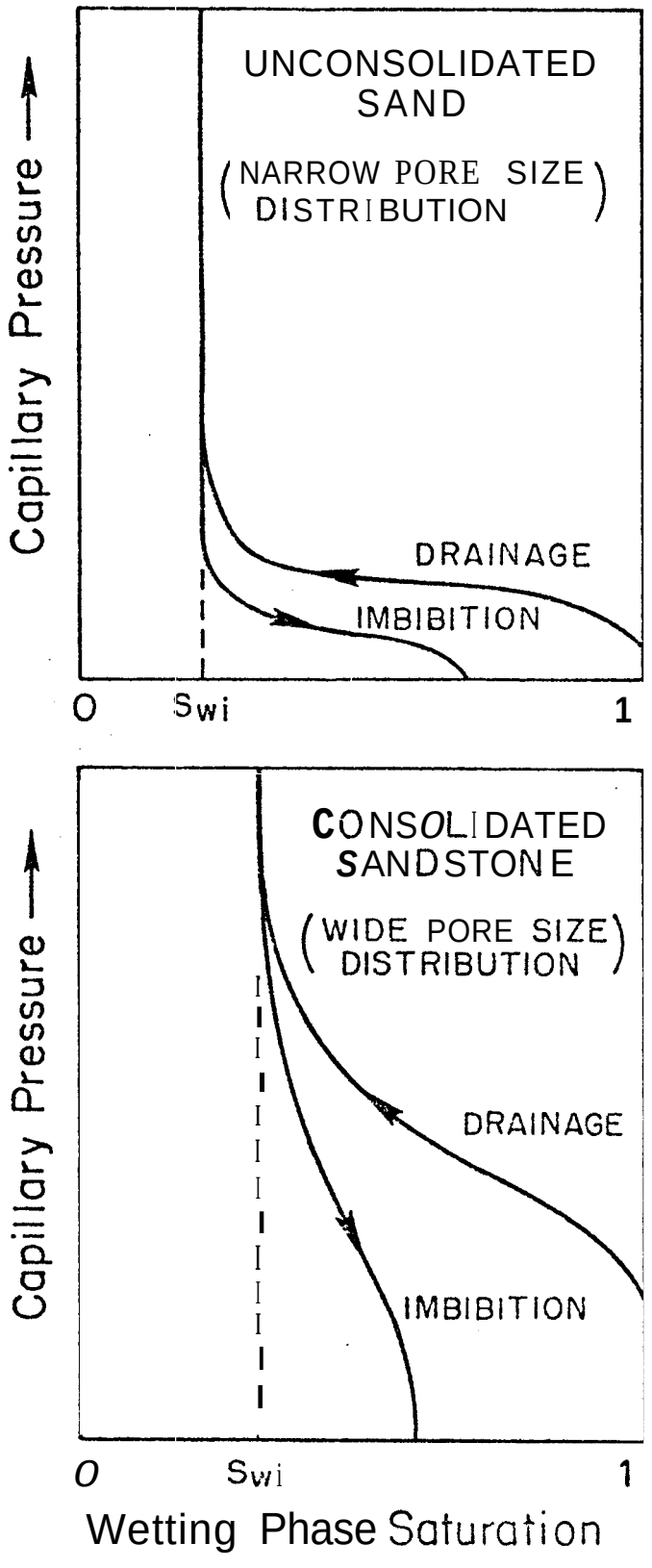

Additionally, temperature effects in unconsolidated and consolidated sands are expected to be different. Sanyal, et al.,[17] hypothesized that, whereas unconsolidated spheres will not change porosity (only bulk volume) with increasing temperature, an increase in temperature in consolidated rock should cause an increase in bulk volume, and a decrease in porosity. This results from the expansion of the cemented grains into the pore space.

As a follow up to the results of Cady[10] and Bilhartz,[14] Strobel[18] investigated the possibility of vapor pressure lowering in consolidated sandstones at high temperatures. Reservoir pressure was graphed versus the measured temperature for the two-phase zone of a reservoir model. The resulting vapor pressure curve for liquid-steam equilibrium in a porous media was compared to similar profiles for planar interfaces, such as Keenan and Keyes.[2] Strobel's figures A12 through A16 appear to indicate the presence of vapor pressure lowering (see Figs. 8 and 9). Each succeeding run, representing decreasing saturation, exhibits a slightly lower curve than the preceding one. This trend appears to be consistent with the results of Calhoun, et al.[8]

However, Strobel[18] acknowledged a number of potential sensing errors in his experiments. In attempting to quantify the approximate extent of the phenomena in his runs, he tried to compensate for each of the more obvious errors. After doing so, he reported a tentative lowering of the vapor pressure curve by $4^{o}F$ to the right (increasing temperature

Fig. 9

EXPERIMENTAL RESULTS FROM STROBEL (Ref. 18)

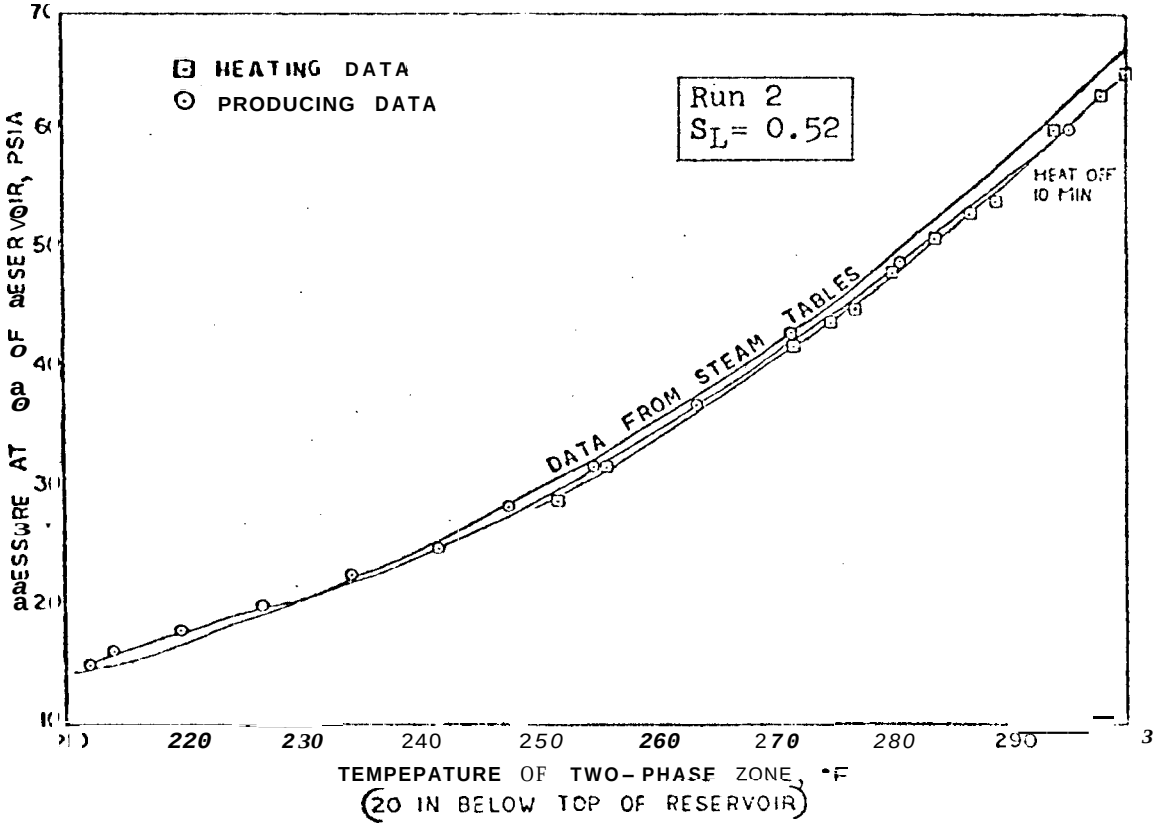

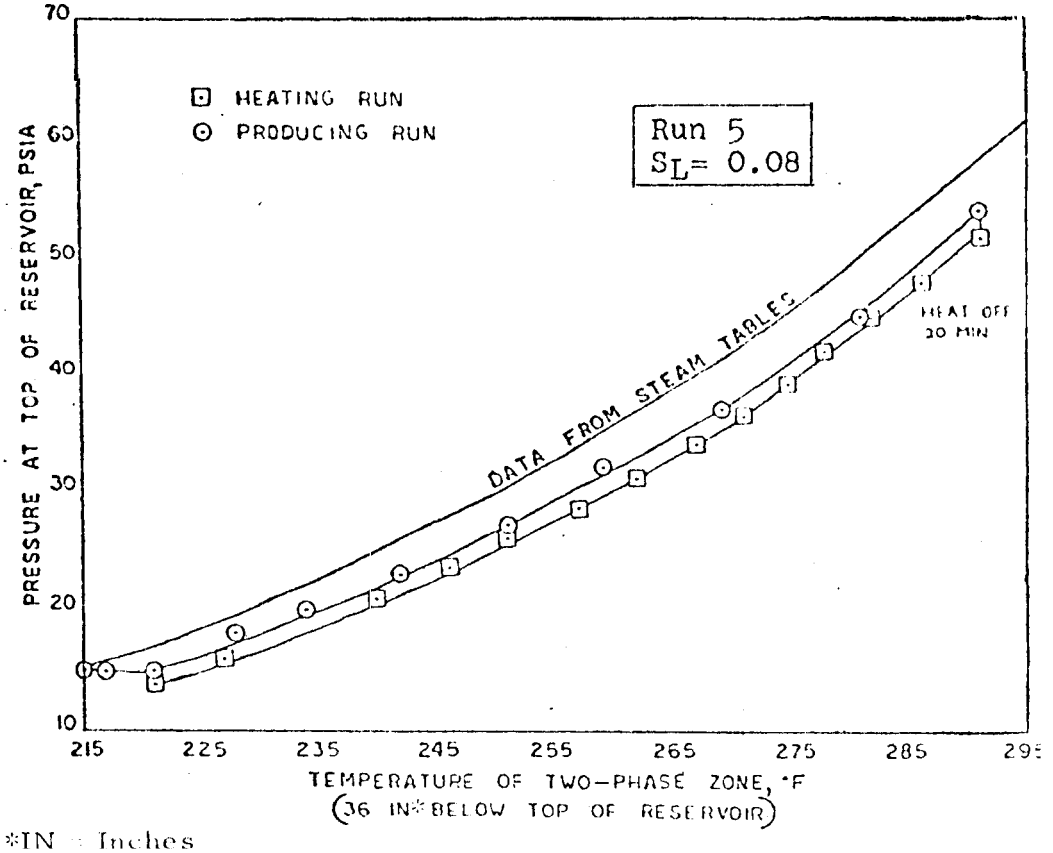

*IN = Inches

for a given pressure) in the 250°F - 280°F range. Such results, though not of a definitive nature, clearly suggest further work on this phenomena in order to establish the validity of the qualitative nature of the findings.

The earlier research in Stanford's Department of Petroleum Engineering in regard to geothermal reservoir modeling was carried out with minimal industrial funding. Most of the funds actually used had been initially earmarked for non-isothermal flow in porous media involved in thermal recovery studies. The only significant geothermal funding was supplied by the Southern California Edison Company. Equipment was built with an emphasis on ingenuity, practicality, and a low budget. The result left much room for improvement in instrumentation as the budget was expanded in the construction of the reservoir model. With the recent financial support from the National Science Foundation, it has been possible to reconstruct the laboratory apparatus with proper instrumentation.

EXPERIMENTAL APPARATUS

A schematic diagram of the experimental apparatus used in this study is shown in Fig. 10. More detailed diagrams of the equipment are discussed later in this section. Figs. 11 through 13 are photographs of the laboratory setup.

A vacuum pump was used to withdraw air from the water source prior to injection in order to eliminate the possibility of introducing dissolved air into the system. While the cold feed water was pumped through the inflow line: and lower shut-off valve into the core, a vacuum was maintainecl on the outflow end of the system to prevent the entrapment of air within the pores. In this way, accurate calculation of the initial liquid pore volume was possible.

The core was contained in a modification of a Hassler-type core holder designed by Marathon Oil Company. The basic core holder (Fig. 14) consisted of an outer stainless steel shell, a Viton sleeve within the shell, the end plugs fitted within the Viton (to seal the core inside from the annulus between the sleeve and shell), and the threaded end caps on the stainless shell. The two caps held the plug at the outlet end and a compression ring at the inlet end tightly against o-seals. The inlet plug was adjustable, sliding through the compression ring, so that the inside face made good contact with the core. The outer shell

Fig. 10 SCHEMATIC DIAGRAM OF EXPERIMENTAL APPARATUS

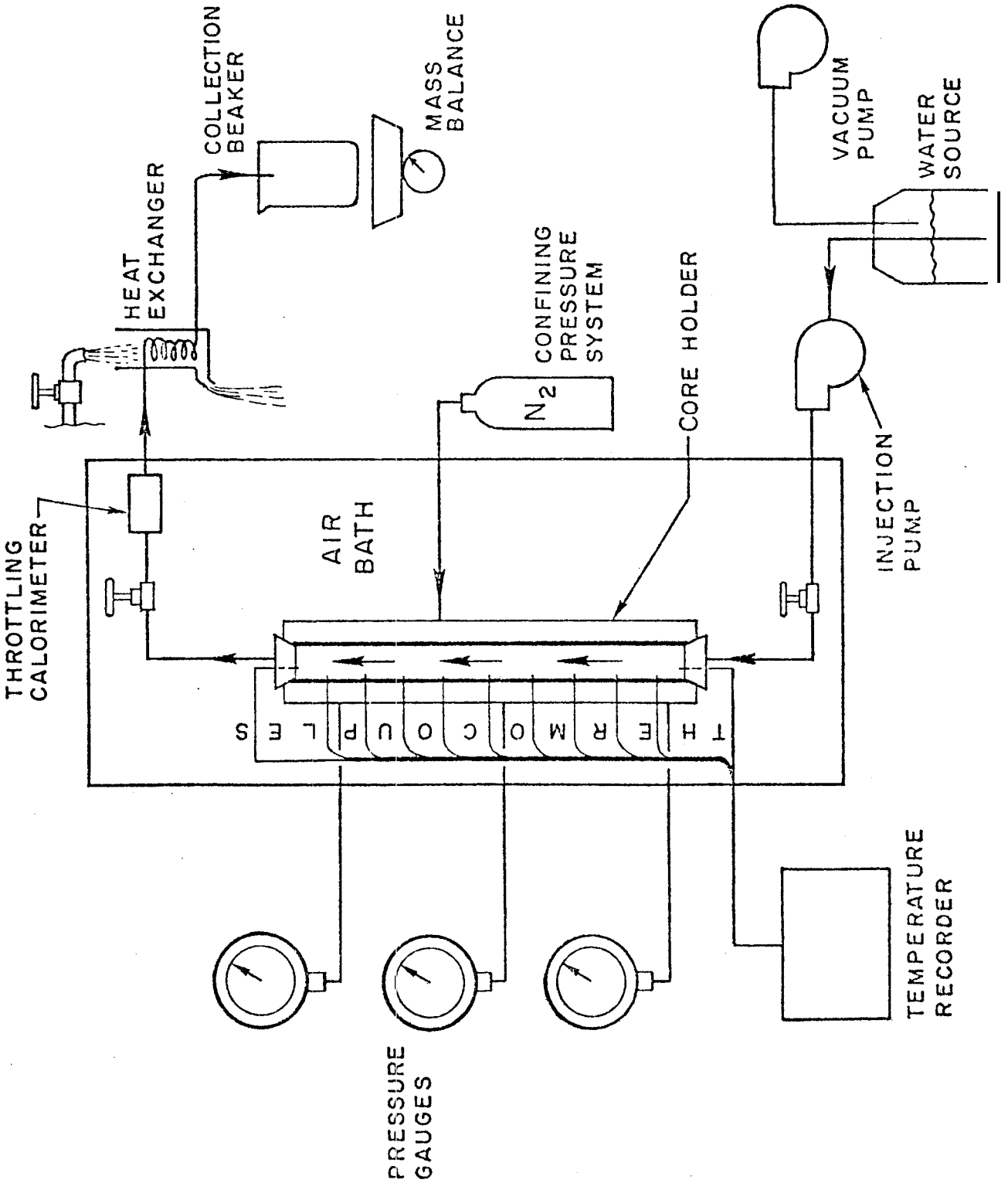

Fig. 11

VIEW OF APPARATUS FROM SENSING/PRODUCTION SIDE

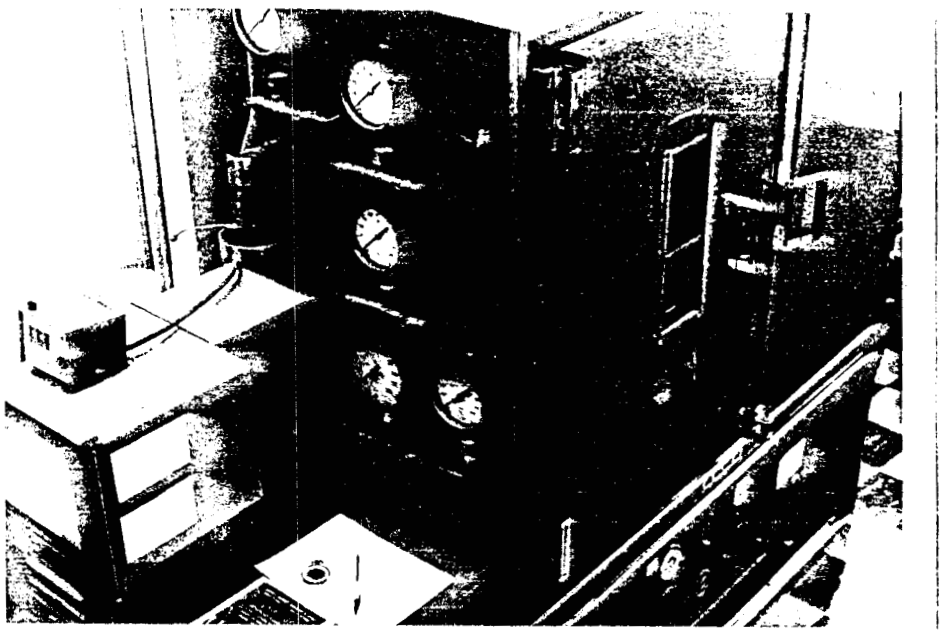

Fig. 12

VIEW OF APPARATUS FROM CONFINING PRESSURE/INJECTION SIDE

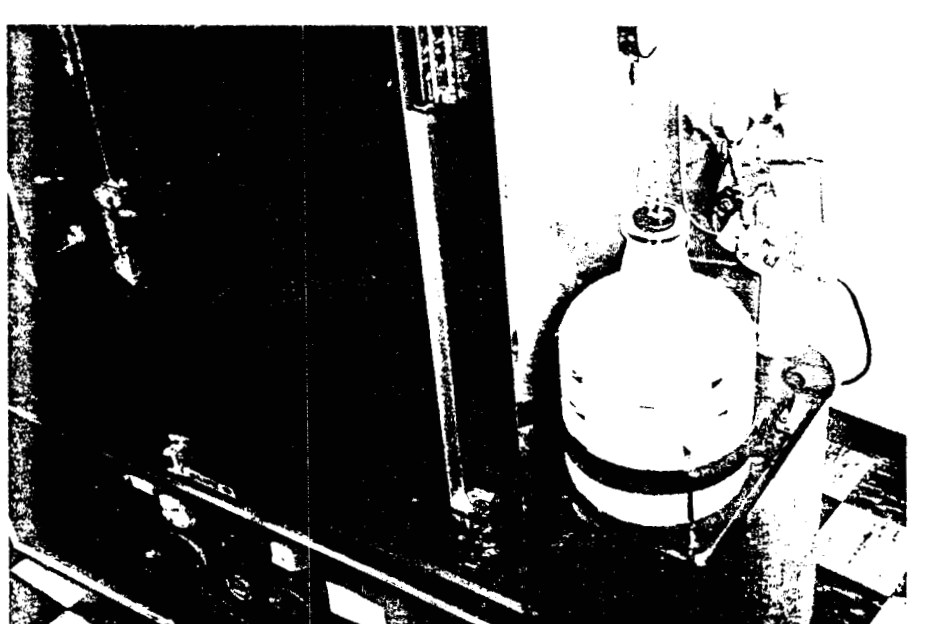

Fig. 13

CLOSE-UP VIEW OF SENSING/PRODUCTION SIDE OF APPARATUS

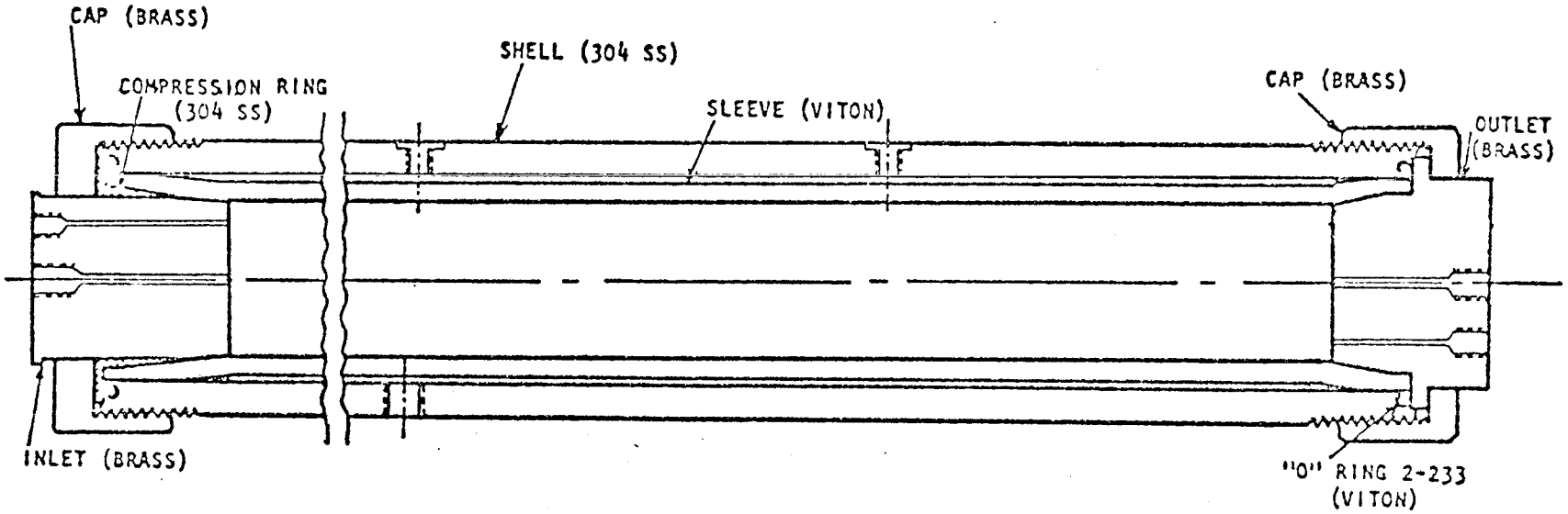

Fig. 14 CORE HOLDER

(FROM ARIHARA, Ref. 19)

measures 26 inches long, with an outer diameter of 3.5 inches. and a wall thickness of 0.438 inches. Confining pressure (analogous to overburden pressure in a natural system) in the form of nitrogen gas within the annulus was applied through a tap in the stainless steel shell. This forced the Viton sleeve to grip the core within tightly, thus sealing off flow along the periphery of the core.

The core holder assembly rested in a vertical position on a metal stand (shown in Fig. 15) within a mechanical convection air bath. With a controlled ambient temperature surrounding the core, accurate measureinents could be made of the heat gain* for purposes of a material-energy balance.[20]

Temperatures were monitored with eleven iron-constantan thermocouples, accurate to $\pm 2^{o}$F, spaced evenly along the core length. Nine were inserted radially into the cylindrical core holder, and two were Located in the end caps. Temperature signals were transmitted to a multipoint recorder. Three of the eleven temperature taps were also utilized for pressure measurements. One-eighth inch lines were run from the pressure taps through the wall of the air bath to pressure gauges accurate to 0. 5 psi. Fig. 16 illustrates the tube fitting assembly utilized for the temperature arid pressure sensing of reservoir conditions through the ports in the shell of the coreholder.

---

*As reservoir temperature dropped corresponding to the pressure decline such that two-phase equilibrium was maintained (while ambient oven temperature was constant), we would observe a heat gain.

Fig. 15

CORE HOLDER ASSEMBLY WITHIN THE AIR BATH

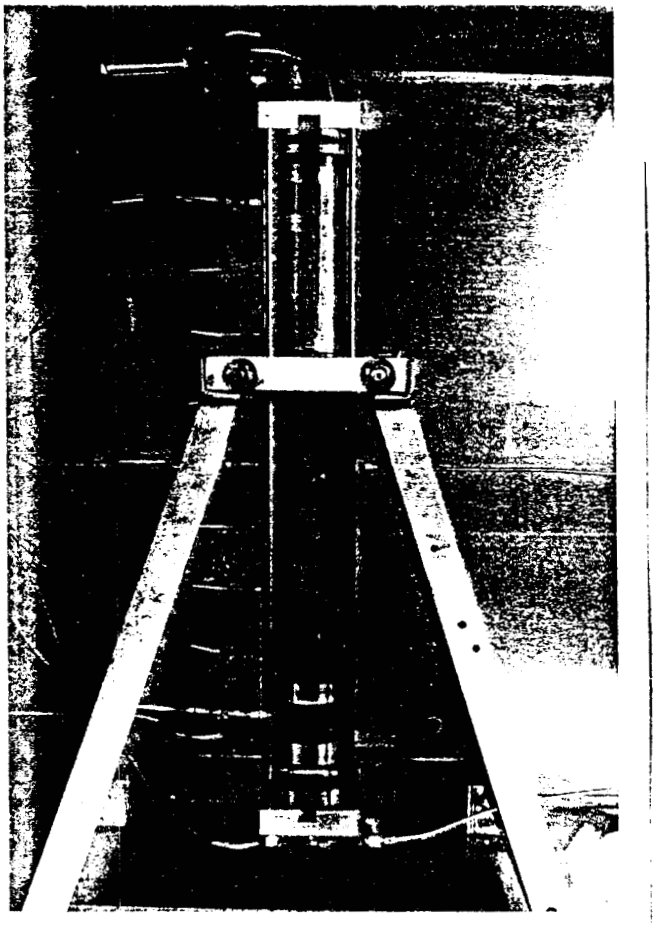

Fig. 16

SWAGELOK TUBE FITTING ASSEMBLY
FOR
TEMPERATURE/PRESSURE SENSING OF CORE

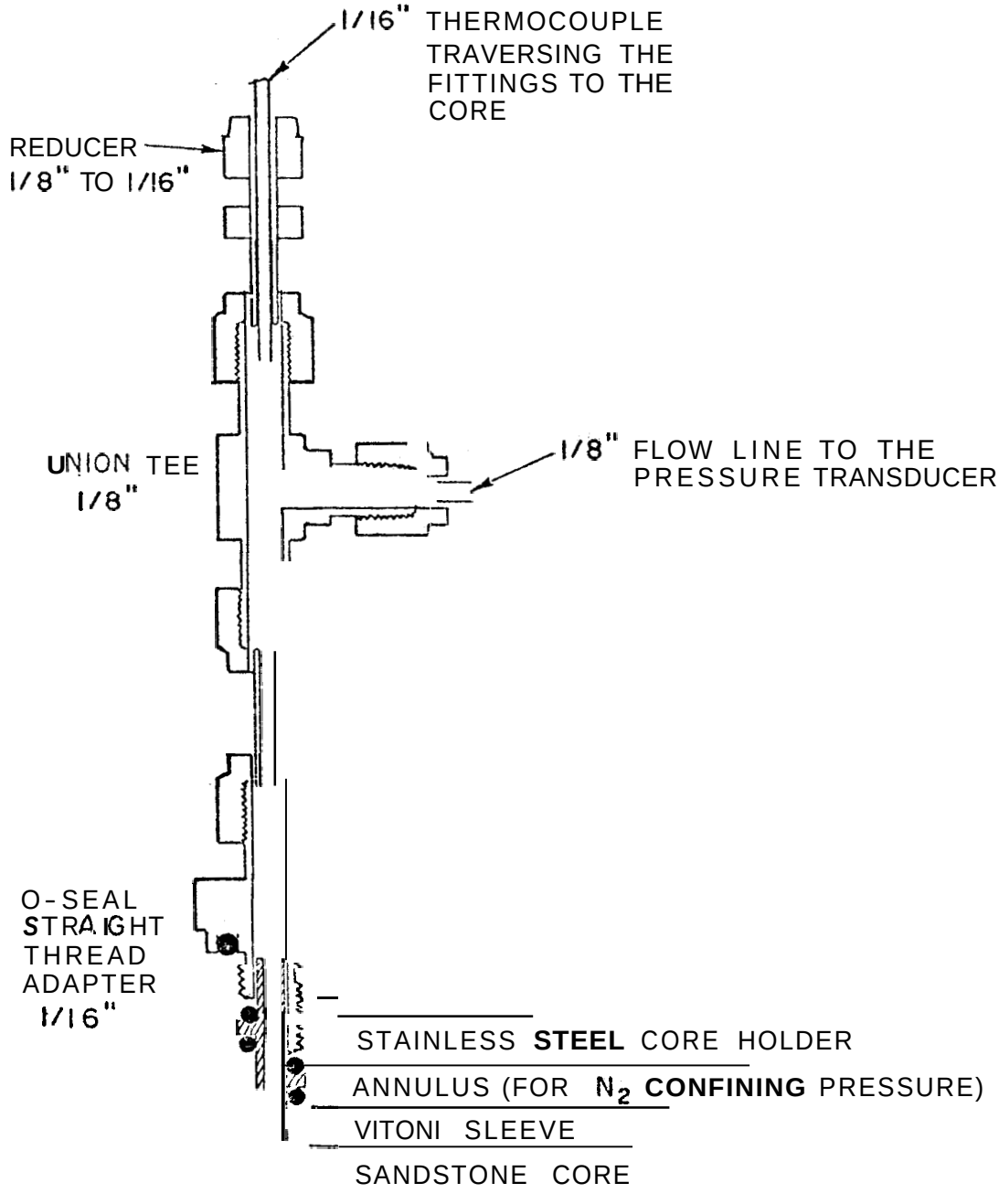

Fluids are produced out of the system from the top through a special metering valve allowing precise control of flowrate. The fluids then enter an adiabatic flow device (shown in Fig. 17). Because of the path of flow, the temperature of the fluid on either side of the inner wall should be virtually the same. This then causes adiabatic conditions (no heat loss) in the center cavity where the incoming fluid hits the wall and reverses flow. Given a single phase fluid in this adiabatic environment, pressure and temperature measurements within the center cavity should yield a reliable value of the enthalpy or heat content of the fluid (Fig. 18). In order to arrive at values as close as possible to the actual enthalpy of fluid in the reservoir, it is important that some type of insulation (asbestos cloth, glass wool, etc.) be wrapped about the production line from the top of the core holder to the calorimeter. In this way, heat gain from ambient air conditions to the fluid would be essentially prevented.

The outflow production valve can be used in conjunction with the adiabatic flow device as a throttling calorimeter setup for the purpose of determining the steam quality of the fluid produced from the top of the reservoir (prior to formation of dry steam cap as system evolves). This is accomplished by throttling the saturated steam from reservoir pressure to atmospheric pressure. If the steam quality in the two-phase mixture from the reservoir is fairly high, this should superheat the steam. In the throttling process, enthalpy is converted into kinetic energy, which is completely reconverted by friction into heat without

Fig. 17 THROTTLING CALORIMETER/ADIABATIC FLOW DEVICE

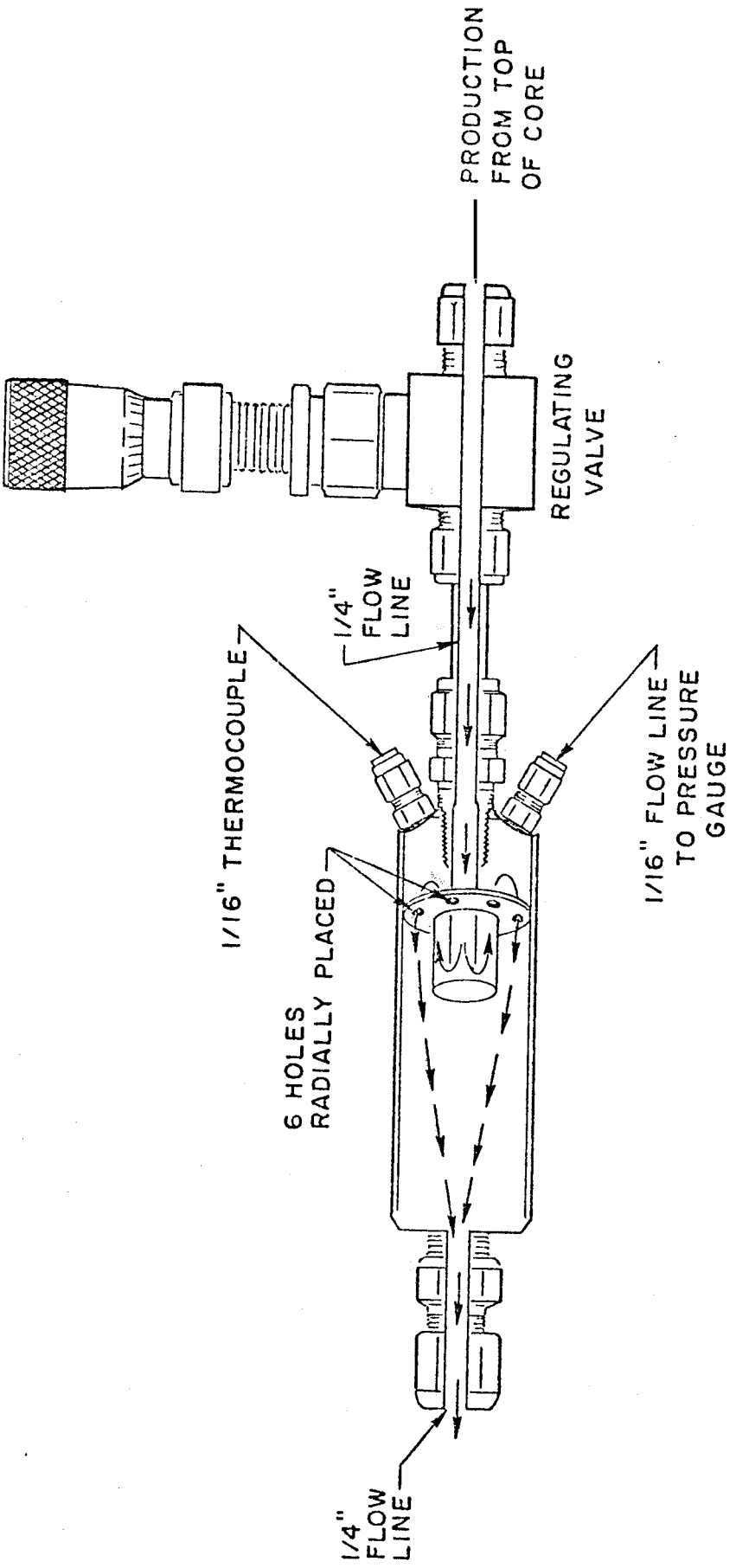

Fig. 18

PRESSURE - ENTHALPY DIAGRAM FOR WATER

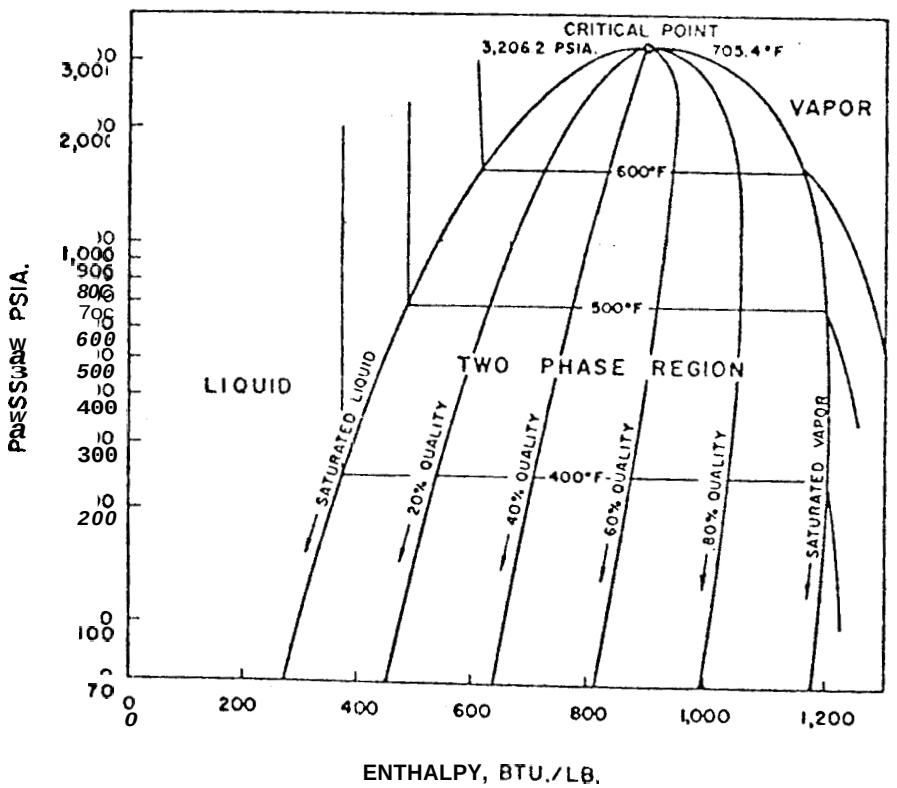

doing esternal work (adiabatic conditions), *so* that enthalpy before and after the throttling has the same value. Then, the enthalpy of the wet steam, h_w, equals the enthalpy of the superheated steam in the calorimeter, h_s. As

$$h_w = h_f + xh_{fg} \quad (4)$$

where

h_f is enthalpy of saturated liquid (BTU/lb)
h_{fg} is heat of evaporation (BTU/lb)
x is steam quality, mass fraction

then

$$h_s = h_w = h_f + xh_{fg} \quad (5)$$

The steam quality of the saturated steam can be obtained from:

$$x = (h_s - h_f) / h_{fg} \quad (6)$$

where

h_s corresponds to the temperature and pressure measured at the calorimeter

h_f and h_{fg} correspond to the temperature and pressure at the top of the reservoir

The fluid then passes along the flow line through the oven walls to the heat exchanger. Here the fluid is condensed as it passes through ten feet of tubing coiled within a cold water bath. The fluid then runs off into a collection beaker resting on a scale, where its total mass is weighed for a check on the energy-mass balance calculations.

Note: For detailed equipment and instrumentation specifications and sources, the reader is referred to Appendix C.

PRODUCTION CHARACTERISTICS OF GEOTHERMAL RESERVOIRS

Before analyzing the operating procedure for the physical model discussed in the previous section, it is helpful to consider the basic phenomena involved in the production of geothermal reservoirs.

The thermodynamic path of production of a geothermal reservoir is dependent upon the initial state of the system. Consider a superheated steam reservoir. It is analogous, in a general sense, to a dry natural gas reservoir in that the production mechanism is the expansion of in-place gas with pressure reduction. As there is no phase change involved in the process, the path of depletion is essentially isothermal, as shown in Fig. 19. Thus, existing petroleum reservoir engineering techniques can be used with relative ease.

In a compressed liquid reservoir, production would be isothermal (expansion of in-place liquid with pressure reduction) until the pressure decreased to the vapor pressure curve. At this point, the liquid would begin vaporizing and the reservoir would become a two-phase system with saturated steam and liquid water. Further production would bc characterized by decline along the vapor pressure curve, the temperature decrease corresponding to the pressure decline upon fluid depletion such that two-phase equilibrium was maintained (Fig. 20). The drive mechanism is similar to that of solution gas drive in a petroleum reservoir.

Fig. 19

THERMODYNAMIC PATH OF PRODUCTION
OF A
SUPERHEATED STEAM RESERVOIR

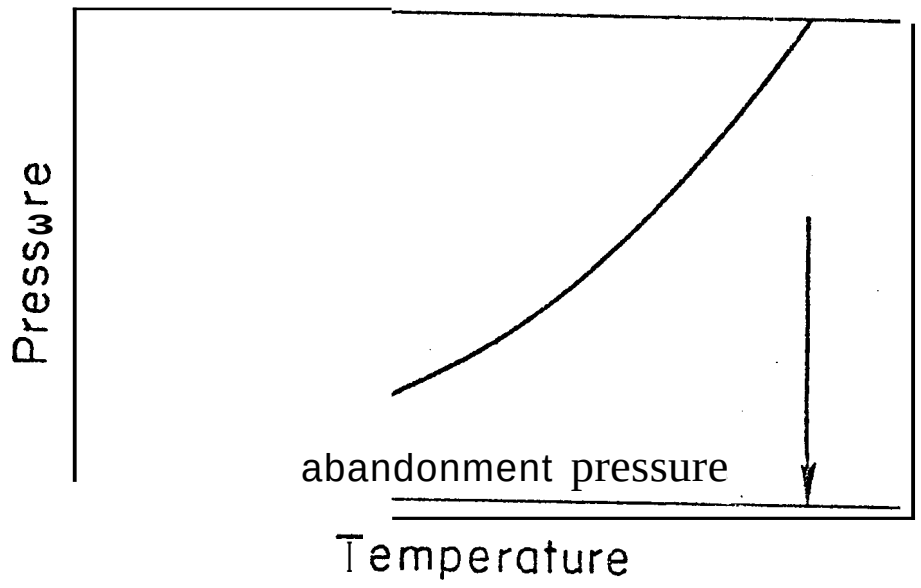

Fig. 20

THERMODYNAMIC PATH OF PRODUCTION
OF A
COMPRESSED LIQUID RESERVOIR

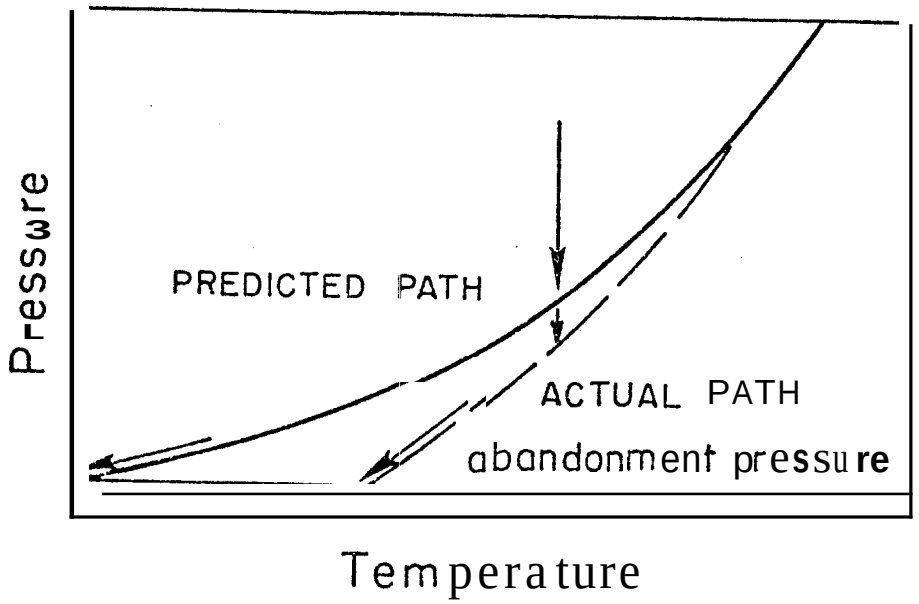

Thus, a knowledge of the thermodynamic path of depletion is essential for production forecasting. For a system initially in the compressed liquid state, this requires an understanding of the thermodynamic relationships governing the vapor pressure curve. Quite obviously, the existence of a vapor pressure lowering phenomenon would result in a lower thermodynamic path of depletion than originally expected (Fig. 20). Thus, at abandonment pressure, the reservoir temperature could be considerably higher than anticipated (depending on the degree of lowering), resulting in an error in predicted energy recovery from the system. The ramifications of such an error could include a serious effect on the overall return on the investment in the producing field.

Upon the transition from a compressed liquid system to a two-phase system, gravity segregation of the fluids can be expected due to the density contrast of the steam and the liquid water. Analyses of reservoir performance indicate that, in many cases, gravity segregation occurs rapidly in two-phase petroleum reservoirs.[21,22] Similar rapid segregation should occur in geothermal reservoirs. An accumulation of steam would gather at the high point of the structure while the liquid drains downward (analogous to the formation of a secondary gas cap in a hydrocarbon reservoir after the gas comes out of solution). Within the upper zone then, gravity drainage would reduce the liquid saturation to the "irreducible" level.[15] The subsequent boiling off of this residual liquid could result in a superheated steam cap. If the vertical extent of this dry steam cap is sizable relative to that section of the reservoir

being observed by producing wells, then it is referred to as a "dry steam field." At some depth, where the vapor pressure corresponding to that level's temperature just exceeds the absolute pressure, saturated steam would be boiling off from the water table.

It should be noted, however, that a dry steam or vapor-dominsteci system (tause the correct terminology in the geologic sense) begins to evolve only in the event that the heat supplied to a two-phase reservoir becomes great enough to boil off more water than is being replaced by recharge (for the physical model used in this study, no recharge was involved for this reason). Because a vapor-dominated system requires a special set of geologic and physical requirements,[23] we can accordingly expect commercially attractive dry steam systems to be rare relative to the occurrence of those that are instead liquid-dominated or two-phase. White[Z4] estimated that liquid-dominated systems were probably over twenty times more frequent than vapor-dominated systems.

If measurements of temperature and pressure in a superheated reservoir indicate conditions relatively close to the vapor pressure curve, it is possible that liquid water coexist in thermodynamic equilibrium with the so-called dry steam. This relates to the presence of vapor pressure lowering when it is, in fact, not expected. With this phenomenon, steam which, in terms of flat interface saturation conditions, falls within the superheated regime, may actually lie on the vapor pressure curve for curved interfaces. Hence, the steam cap may not be 100% steam, as is

commonly taken for granted. An important clue to the presence of liquid would be non-isothermal pressure depletion.

In regard to the various types of geothermal reservoirs, the liquid-dominated or two-phase systems contain substantially more available energy than those that are vapor-dominated (superheated steam). Ramey, et al.,[25] noted that, although the latent heat of vaporization of steam is high with respect to the sensible heat of liquid water of the same temperature, the dense liquid has a much larger mass, thus providing greater available heat. But, even more significantly, the mass of the rock will always be much greater than that of the total fluid and thus the rock contains most of the available heat. This thermal energy can only be recovered from the rock by a production process that reduces the temperature of the rock significantly. As the flashing of liquid water to steam upon pressure reduction is a non-isothermal process, the recovery of this energy is possible in the case of a two-phase reservoir.

Because of this consideration, from an energy recovery standpoint, the liquid-dominated systems are more interesting targets (of course, heat scavenging, in the form of a cold water injection program, would substantially boost energy recovery in the vapor-dominated systems). However, due to production and environmental considerztions, steam reservoirs are still thought of as more attractive to development groups. The total fluid cart be piped directly to the turbine and fluid disposal of condensate is minimal. In contrast, the exploitation of liquid-dominated reservoirs involves steam-water mixtures requiring mechanical separation and considerable injection.

OPERATION OF THE PHYSICAL MODEL

Initially, water was injected into the core to attain 100% liquid saturation. At the same time, a vacuum was maintained from the outflow end in order to prevent the entrapment of air in the pores. The inflow and outflow valves at either end of the core were then c osed, shutting in the system. As the air bath heated up to operating temperature (300^{o}F), the liquid expanded, forming the desired compr ssed liquid reservoir.

In order to permit direct observation of the production characteristics of the various forms of geothermal reservoirs, it is necessary to deplete the system as closely as possible with a hydrostatic pressure gradient. If the production out the top of the core resulted in a considerable pressure drawdown throughout the system, the scale of the model would be closer to the vicinity of a wellbore than that of a vertical section of a gravity segregated geothermal reservoir.

While pressure and temperature along the length of the core were recorded, the production valve at the top was opened and the reservoir depleted to atmospheric conditions. In a natural geothermal field, this would normally be the terminal situation. However, at this point the reservoir would still retain a high liquid saturation. As mentioned earlier, in order to observe the vapor pressure lowering phenomenon, liquid saturation must be decreased to low levels.

For this reason, a cyclical procedure was used. Following each production run, the outflow valve was again closed. In this way, the reservoir temperature was allowed to re-equilibrate with the ambient temperature of the bath. With this reheating of the core, the liquid once again expanded. However, the system, having been partially depleted by production, would not expand to a degree sufficient to suppress boiling.

This cyclical production and reheating of the reservoir without liquid recharge is somewhat analogous to the evolution of a superheated steam system, discussed in the previous section. Each cycle was conducted at a lower liquid saturation level than the preceding run. Gravity drainage would reduce liquid saturation in the upper portion to "irreducible" saturations beyond which the boiling off of this would result in a dry steam cap. The liquid remaining after each run migrated toward the lower portion of the core, confined to an ever smaller pore volume during succeeding runs. As this migration of liquid downward will, for a time, maintain the liquid saturation in the two-phase zone above the levels at which vapor pressure lowering is expected, the core must be nearly dry before the effect can be espected.

Precise temperature and pressure measurements within the two-phase zone (identified from a temperature profile of the core) during both the production and heating cycles should define the vapor pressure curve for water within the porous media at various levels of liquid saturation. From this data,, comparison can be made with steam table,

data to ascertain whether or not vapor pressure lowering due to capillary pressure effects in a porous media is an observable phenomena.

DESIGN CONSIDE€7ATIONS INVOLVED IN CONSTRUCTING THE APPARATUS

A great deal of time was devoted to rendering the system operational through the necessary modifications. In many cases, the need for these changes was not apparent until test runs were made with the esisting setup. A brief description of the design considerations follows.

Confining Pressure

This was the most difficult problem to overcome. The general design of the Hassler-type core holder required considerable modification.

In order that the Viton sealed off the nitrogen in the annulus from the core, it was very important that the sleeve reached as far up onto th lip of the end plugs as possible. It was found that the length of the Viton sleeve was irreversibly reduced to a small degree when compressed in the process of ramming the core into the tight fitting sleeve. For this and other reasons, it is recommended that the Viton sleeves be ordered in longer lengths than needed, then be cut to the desired length when the core is installed and the end plugs' position noted. In the case of sleeves that were marginally long enough, expansion-contraction from heating runs and snbsequent cool clown resulted in the leakage of nitrogen into the core through the end piece contacts after initial pressure-tight runs.

Smooth surfaces are essential for the Viton sleeves. Ridged surface Viton, such as received in early purchasing, caused great problems with nitrogen leakage into the core. Silicone vacuum grease helped considerably in sealing any surface of contact.

A piece of one-eighth inch diameter tubing, sharpened on a file, was used to drill the holes through the Viton for the pressure-temperature taps. Great care must be taken in centering the holes directly below the threaded ports. For this reason, the holes must be drilled through the Viton after the core has been placed within it. Otherwise, the Vitoa may he shifted by the placement of the core.

The confining pressure should just exceed the pore pressure. Large pressure differentials between the annulus and the core could promote leakage. Adjustments to the confining pressure should be gradual. The rapid release of nitrogen from the annulus can actually suck Viton into the tubing line that conducts nitrogen into and out of the annulus, blocking the line. The rapid increase of confining pressure can tear O-rings from the small brass taps that seal the nitrogen off but allow reservoir sensing.

Whereas it is difficult to seal nitrogen gas in the annulus with nine sensing taps to the core as well as the two end pieces, there is a distinct advantage. In the event of a gas leak to the core, the gas can be removed by injecting water and evolving superheated steam in the core. Nitrogen is commonly in the core and liner anyway for leak detection as the "snoop" leak detector solution works only for gases.

The use of oil, for example, for the confining pressure would be disastrous in the event of a leak to the core, introducing surfactants into the system. The core would be ruined for the purposes of the study's objectives.

The small brass fittings which sealed off the nitrogen gas from the pressure taps into the core were difficult to work with. The critical point was the amount of clearance between the outer surface of the Viton sleeve and the inner surface of the stainless steel shell. Under normal conditions, the brass fittings each had two small O-rings, one for the contact with the base of the o-seal straight thread connector and one for the contact with the surface of the Viton sleeve. However, if the clearance is tight, expansion of the Viton in the initial heat up of the core may force the upper O-ring into the threading fitting, tearing it. This situation is apparent when the confining pressure holds tight at room temperature but leaks out immediately upon the heat up. When Viton sleeves have been used in earlier runs, the bottom O-ring leaves a deep impression in the sleeve. Subsequent attempts at holding the confining pressure may fail until a second O-ring is added to the bottom part of the brass fitting to snug up the fit.

Whereas the present arrangement with the brass fittings has, at times, been successful in holding the confining pressure, this accomplishment has always been sporadic. This seems to be, at least in part, due to the ever changing amount of clearance in the annulus. It is recommended that some type of adjustable fitting be designed.

Thermocouples and Temperature Sensing

The one-sixteenth inch diameter thermocouples used in the setup are very susceptible to damage and must be handled with care. The continua1 insertion and withdrawal of the thermocouples into ancl out of the core (that is required whenever the confining pressure leaks into the core) compounds the problem.

When the stainless steel ferrules are crimped too tightly around the thermocouples, the continuity of the MgO powder insulation may be broken. In this event, the temperature reading would be made at this point. That is, the temperature read would be the ambient temperature rather than the core temperature at the tip of the thermocouple where the sensing is supposed to be. This problem was alleviated by switching to teflon ferrules.

Continual bending of the thermocouple will ultimately break the sensing wire, causing an open circuit. Due to the spatial limitations in the oven, there is little vertical clearance at the top and bottom of the core holder. For this reason, the thermocouples placed in the end pieces must be bent as they are inserted. The regular loss of thermocouples can only be avoided by switching from one-sixteenth inch to one-eighth inch thermocouples.

Whereas mechanical contact of the tip of the thermocouple with the core may be sufficient, it is best to drill into the core for the thermo-couple setting in order to avoid sensing some average of ambient and core

temperature. For consolidated cores, it is necessary to use carbide drill bits. Because of the brittle nature of the bits, a small hand drill was used.

Pressure Sensing

The pressure gauges used in the test runs were initially planned only as a crude check on the output of the pressure transducers. However, due to unforeseen equipment problems and subsequent delays in shipping replacements, both the pressure transducers and recorder were to pressure, even at high levels of resolution. Factory specifications set combined error due to non-linearity and hysteresis at 0.5% of full

The pressure recorder offers a great deal of versatility with regard to handling the transducer output. The full scale span on the printout chart can be varied from 100mV (maximum output of the transducer, roughly equivalent to 300 psi) down to 0.5mV (for a resolution of 0.015 psi per chart paper division). With the substantial zero suppression capability of the recorder, the full scale can be displayed either as 0 to 50mV, but also as 50 to 50.5mV.

This arrangement will allow high precision in the measurements made with the pressure sensing system. The only uncertainty with regard

to the Observation of reservoir behavior lies in the ± 2°F error range of the thermocouples. If the lowering of the curve results in a temperature shift greater than 2°F for a given pressure, then vapor pressure lowering can be reported as essentially certain. If not, then a tighter core might be used to introduce more suitable conditions for the observation of the phenomenon.

Because the reservoir system is closed, once fluid has been admitted to the transducer, the zero setting on the recorder cannot be checked during the runs. For this reason, only one zero setting is possible on the recorder for the four transducers (each with different outputs at zero pressure). Thus, the calibration of all four transducers should be based on the zero setting of one transducer (set on the smallest span, 0.5mV, *so* that slight errors in the setting will be lost with span changed). This transducer is then the basis for setting the zero for experimental runs.

Injection Setup

As the model was designed for batch-type experiments, the function of the pump was simply to saturate the core prior to the actual experiment (the production-heating cycling of the reservoir without recharge). For this reason, two pieces of equipment commonly found in flow systems were Left out. Experience has shown that this point might be reconsidered in future work. The measurement of permeability and the overall heat transfer coefficient both require flowing experiments. Their determination is important.

An accuniulator is needed downstream of the pump in order to eliminate flow pulsations resulting from the working action of the pump's diaphraghm. Without it, accurate pressure drop determinations are difficult. In addition, it becomes difficult to set the confining pressure with the rapid fluctuations in pore pressure.

Present flowrate is determined by measuring production into the collection beaker with time. A flowrate meter might serve as a check on the values obtained in this manner.

Heat Exchanger

The heat exchanger was designed so that the cooling water was introduced at the bottom and removed by runoff at the top. In this way, the warmest water was always removed, allowing for maximum heat exchange between the hot produced fluids in the outflow line and the cooling fluid.

It was critical that the length of coiled production line in the cooling bath be long enough to allow complete condensation of the produced steam and yet not *so* long as to cause a great time lag between the actual production from the top of the core and its measurement at the scale.

Production Line

In order to avoid plugging of the flow line due to mineral deposition, the lines used from the top of the core to the calorimeter were one-quarter inch in diameter.

GEOCHEMICAL CONSIDERATIONS

For the purpose of investigating the effect of interfacial tension on the vapor pressure of water, distilled water was used in the laboratory system. In this way, the introduction of surfactants, which might lower the interfacial tension, was avoided. However, because of the chemical disequilibrium between the distilled water and the minerals in the sandstone, dissolution had to be expected. The high temperature level at which the system was maintained promoted a tendency toward chemical equilibrium as the rates of reactions were substantially increased. Further, the very nature of the experiment (repeated cycles of production and reheating without recharge) with the long residence times of the water in the core allowed for an increasing tendency toward equilibrium with time.

This bears a strong similarity to the evolution of brine in natural systems. Isotopic analyses by Craig[26] demonstrated that the source water of most geothermal systems is, to a great extent, the local meteoric water of the area. The deuterium contents of most thermal waters is nearly identical with that of the surface recharge water of the area while the O^{18} contents are higher, the result of high temperature isotope exchange between the water and rocks.

The chemical composition of most thermal waters appears to be, to a large part, dominated by water-rock interaction. This was clearly

demonstrated by the experimental studies of Ellis and Mahon.[27,28] They noted that chemical equilibria between rock minerals and aqueous solution were responsible for the compositions of thermal water and that the concentrations of the major solub e elements were controlled largely by temperature dependent reactions minor constituents would obviously be controlled by the available supply in the source rocks).

Perhaps the best approach toward an investigation of the sole effects of interfacial tension on the vapor pressure of water would be the use of Al_2O_3 beads to form an essentially non-reactive porous media. Otherwise, the temperature level (300°F) is such that water-rock interaction will always produce a brine solution to some degree in non-recha ge or batch-type physical modets. Boiling will, in fact, result in increased salt concentrations in the liquid as the steam/liquid water ratio of the system rises with pressure decline. However, calculations concerning the magnitude of vapor pressure lowering expected due to interfacial tension effects (shown in an earlier section) indicate that the expected lowering due to salts in solution[29,30] will be significantly less. But unlike interfacial tension effects, which cannot be expected until low volumetric liquid saturations have been reached, salts effects could be significant earlier.

Silica deposition is probably the most significant process due to the ready availability of silica to solution from quartz in the sandstone core. The existing data on the compositions of hot spring solutions and

the solubilities of silica phases strongly suggest that the amounts of silica in solution are controlled by the solubility of quartz at depth (and not of amorphous silica, the precipitated phase).[31] The solubility of quartz increases rapidly with temperature. At 300°F the solubility of quartz in liquid water in the presence of water vapor is about 170 parts per million.[32]

Any calcite precipitation will probably be the result of the lowering of the partial pressure of CO_2 in the system. As the result of rapid vaporization upon sudden pressure reduction, much CO_2 is selectively lost to the vapor phase. The carbonate equilibria is shifted and bicarbonate ion, HCO_3^-, is converted to carbonate, $CO_3^=$ (increasing the pH of the solution), resulting in the deposition of calcium carbonate, $CaCO_3$.

The importance of considering the existence of brine within the core was emphasized in one of the early test runs. Distilled water was injected into the core and the system was heated up (for approximately seven hours), resulting in a compressed liquid reservoir. Fluids were then produced for several hours while the system remained within the compressed liquid regime (Fig. 21). For the duration of this period, the boiling front remained just within the production port of the end piece, this being the location of the pressure drop from reservoir to atmospheric pressure. The rapid eruption of steam within the port continued to concentrate the water's non-volatile constituents in the remaining liquid phase until their solubilities were exceeded and they were deposited along the

Fig. 21

EXPERIMENTAL DATA - SCALING RUN
THERMODYNAMIC PATH OF PRODUCTION

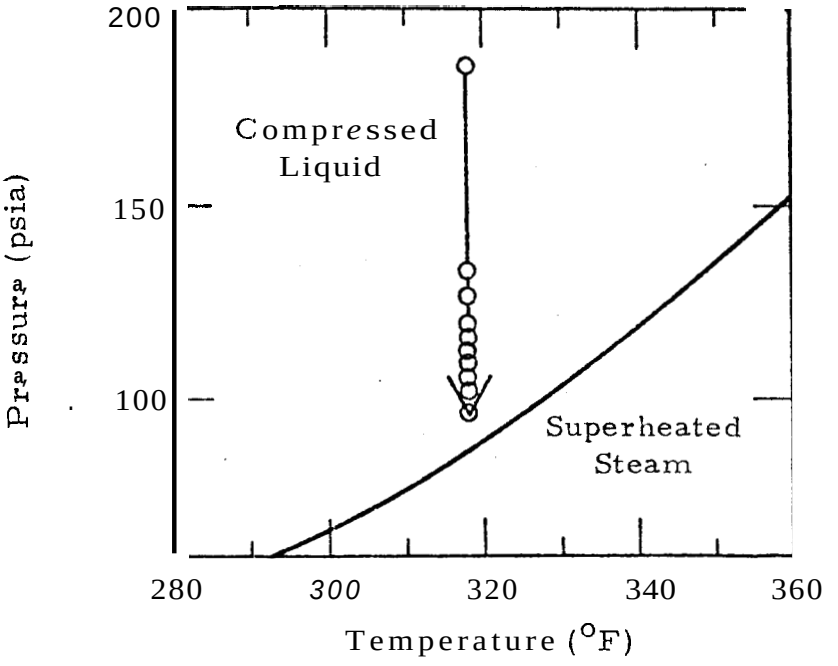

Fig. 22

EXPERIMENTAL DATA - SCALING RUN
CUMULATIVE PRODUCTION AND RESERVOIR
PRESSURE AS A FUNCTION OF TIME

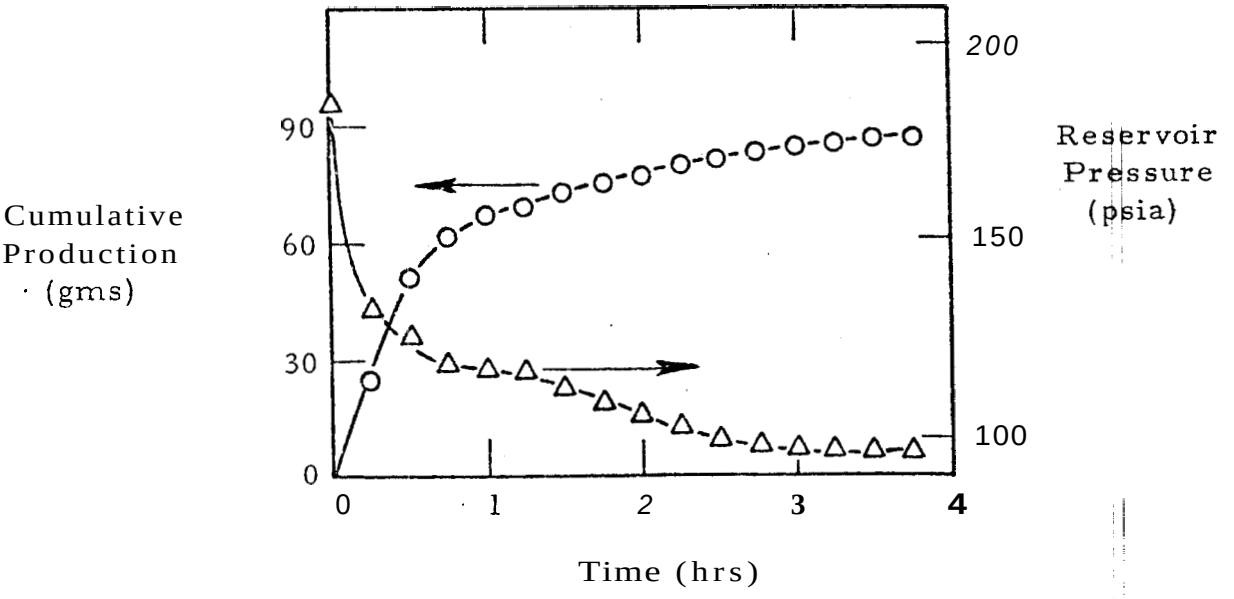

of the port. The effect of this continuing deposition upon the production of fluid and the pressure decline in the reservoir is shown in Fig. 22. Ultimately production ceased and reservoir pressure attained a static level.

Upon disassembling the core holder, the one-eighth inch diameter production port was discovered to be completely plugged with a fine yellow powdery substance. An x-ray diffraction sweep showed the low broad hump which characterizes amorphous material. However, minor peaks seemed to indicate the possible presence of silica and some type of calcium sulfate. In order to more clearly define the nature of the amorphous substance, a microprobe analysis was run on a collected sample.[33] The results are shown in Table 2.

A net reaction cannot be deduced only from the mineralogy of an alteration/deposition assemblage or only from the composition of water flowing from the core. Both are necessary. Further, the microprobe analysis is only an elemental analysis. As the substance was amorphous, the results of the diffraction study were nebulous.

In a general sense, it appears from Table 2 that the deposited Substance consisted mainly of silica SiO_2, anhydrite $CaSO_4$, fluorite CaF_2, and some kind of carbonate, calcite $CaCO_3$, dolomite $CaMg(CO_3)_2$ or magnesite $MgCO_3$. This, of course, represents speculation. Elements in minor quantities were ignored and the semi-quantitative nature of the analysis makes any stoichiometric calculations difficult, if not impossible.

Table 2

MICROPROBE ANALYSIS

Oxygen, O	20 - 30	%
Calcium, Ca	18 - 20	%
Magnesium, Mg	13 - 15	%
Silicon, Si	11 - 13	%
Sulfur, S	3 - 4	%
Fluorine, F	3 - 4	%
Potassium, K	0.5 - 0.7	%
Aluminum, Al	0.2 - 0.4	%
Manganese, Mn	0.25 - 0.35	%
Lead, Pb	0.15 - 0.25	%
Chlorine, Cl	0.1 - 0.2	%
Iron, Fe	0.1 - 0.15	%
Phosphorous, P	0.5 % (possibly)	
Sodium, Na	possibly, but too much interference	
Carbon, C	too light an element for detection	

Brass Derivatives

Zinc, Zn	3 - 4	%
Copper, Cu	.7 - 1.5	%
Total	72.60 - 94.95	%

The data exemplifies the degree to which leaching can occur in rock/hot water interaction. Berea sandstone is a relatively immature fine-grained sandstone with a high percentage of clay material and kaolinite replacement of feldspars (20%). The quartz (about 60% of the rock volume) is an unlimited source of silica. The feldspars (in minor amounts--less than 5%) would release calcium, sodium, and potassium. The main calcium contribution would probably be from the abundant amount of calcite (10%) in the sandstone. The clays are a possible source for just about anything. The presence of sulfate could be attributed to the oxidation of pyrite (some of the opaque minerals observed in thin section may have been pyrite).

The virtual absence of the element chlorine (0.1 to 0.2%) is puzzling. Chloride is, in fact, the single most critical constituent in distinguishing hot-water from vapor-dominated geothermal systems.[23] The chloride content of most rocks is easily leached by high temperature water and most metal chlorides are highly soluble in liquid water.[27,28] As the common metal chlorides have negligible volatility even at extremely high temperatures and are not soluble in Low pressure steam, chlorides should be increasingly concentrated at the boiling front. The only possible explanation seems to be that chlorine was present in the source rock in minute amounts. Certainly the volcanic rocks associated with many geothermal systems are better source rocks for chlorine.

To counteract this scaling problem--the same problem which has plagued the early development of brine fields--the production port was

widened to a one-quarter inch diameter. Also, as the production data clearly verified the isothermal path of production of a compressed liquid reservoir (Fig. 21), it was decided that the initial state not be set nearly as far above the saturation curve in future runs.

It should be pointed out that this same phenomenon also occurs within the flow channels of a porous media. A sudden pressure drop may be due to a sudden widening after a tight flow constriction. Other possible causes of precipitation might include the reduction of the hydrostatic head, decreasing the absolute pressure on the liquid to the point of allowing vaporization to begin or the mixing of hot brine with cooler downward-flowing water. All of these processes may help to originate an effective cap rock in a portion of a permeable formation. This then forms a trap for the convection currents of meteoric water heated at depth and the hydrothermal system may evolve into a self-sealed geothermal system.[35]

The present laboratory setup offers innumerable possibilities for future geochemical reservoir research. Among the more interesting to the reservoir engineer is the evolution of the content of various volatile constituents within the developing dry steam cap. For example, Celati, Ferrara, and Panichi[36] reported extremely high concentrations of boron in early steam production at the Larderello Field in Italy followed by a rapid decrease thereafter. Finlayson and Mahon[37] correlated increases

in the CO_2/H_2S ratio in the Broadlands Field in New Zealand with discharge enthalpies. Ellis[38] and Mahon[39] had earlier done similar work at Wairakei in New Zealand.

OVERALL HEAT TRANSFER COEFFICIENT FOR THE CORE HOLDER

If we assume a steady state temperature distribution in the core, then:

Heat into the core - Heat out of the core = Heat transferred between the core and its surroundings (7)

If we further assume that U, the overall heat transfer coefficient (BTU/hr - ft2 - ^{o}F), is not a function of temperature (a good assumption for steady state), then, from basic heat transfer, we know that:

$$\text{Heat transferred} = \int U (T_{\infty} - T_f) \, dA \qquad (8)$$

where

T_{∞} is ambient temperature (^{o}F)
T_f is flowing temperature in the core at various points along the length (^{o}F)
A is cross-sectional surface area (ft2)

Note:

$$dA = 2 \pi R \, dx \qquad (9)$$

where

R is the radius of the core system (ft)
($2 \pi R$ is, thus, circumference)
x is distance along the core length (ft)

Now Q, the heat flow in or out of the core (BTU/hr), can be represented as follows:

$$Q = q \rho C \Delta T \qquad (10)$$

where

q is the volumetric liquid flow rate (ft^3/hr)
ρ is the density of the liquid (lb/ft^3)
C is the specific heat of the liquid (BTU/lb - ^oF)
ΔT is the temperature gradient along the core length (^oF)

Substituting the appropriate expressions into equation (7), we obtain:

$$m C (T_{in} - T_{out}) = 2 \pi R U \int_0^l (T_\infty - T_f) dx \qquad (11)$$

where

m is mass flow rate (lb/hr)
$(m = q \rho)$

Rearranging equation (11) for U, we get:

$$U = \frac{m C (T_{out} - T_{in})}{2 \pi R \int_0^1 (T_\infty - T_f) dx} \qquad (12)$$

We can evaluate the integral along the length of the core using Simpson's Rule.

The overall heat transfer coefficient was measured by injecting cold water into a hot, dry, isothermal core equilibrated with the air bath's ambient temperature, The development of the temperature-distance profile with time is shown in Fig. 23.

With a constant flowrate maintained throughout the run, cold liquid water entered the lower end of the core and moved up the length, gaining heat from the rock as it passed through the pore channels. With longer distances traveled up the core, greater contact with the rock resulted in more heat transfer and higher temperatures. At some point, the liquid started boiling--with the lower pressure and the higher

Fig. 23

EXPERIMENTAL DATA - INJECTION INTO HOT DRY CORE
TO OBTAIN OVERALL HEAT TRANSFER COEFFICIENT
TEMPERATURE AS A FUNCTION OF DISTANCE IN RELATION TO TIME

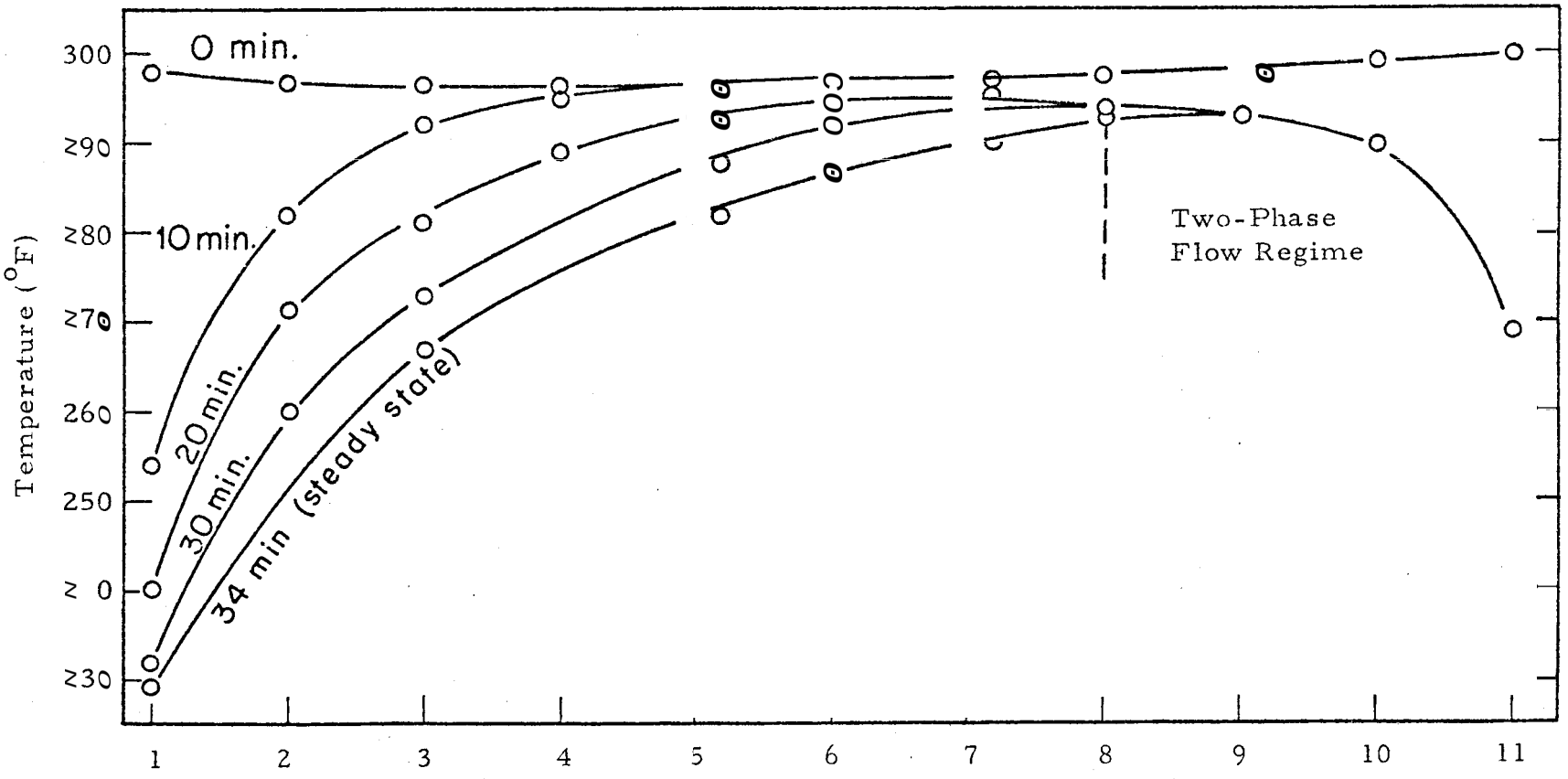

temperature--flowing through the rest of the core as a two-phase mixture of saturated steam and liquid water.

The temperature-distance profile of the single phase region continued to drop with respect to the initial core temperature until steady state was attained. At this point, the temperature profile was fixed with time as the heat flow into the core by radial conduction equaled the heat flow up the length of the core by mass transport. From this steady state profile, the overall heat transfer coefficient was calculated (Table *3)*.

Table 3

CALCULATION OF OVERALL HEAT TRANSFER COEFFICIENT

Thermo-couple No.	Distance from inlet (inches)	T_f (°F)	$T_\infty - T_f$ Difference from 300°F Ambient Temp (°F)	Multiplication Factor (using Simpson's Rule)	
1	0	229	71	x 1	= 71
2	1	2.61	39	x 4	= 1/56
3	2	267	33	x 2	= 66
4	3	275	25	x 4	= 100
5	4	2.82	18	x 2	= 36
6	5	2.87	13	x 4	= 52
7	6	2.90	10	x 2	= 20
8	7	293	7	x 4	= 28
9	8	293	7	x 1	= 7
					$\sum$ = 536

Using Simpson's Rule,

$$\int_0^1 (T_\infty - T_f)\, dx = h^*/3 \left[T_1 + 4\, T_2 + 2\, T3 + \ldots + 4\, T_8 + T_9 \right]$$

$$= (0.2188 \text{ ft}/3)\ (536^\circ\text{F})$$

$$= 39.08^\circ\text{F} - \text{ft}$$

$$U = \frac{m\, C\, (T_{out} - T_{in})}{2\, \pi\, R \int_0^1 (T_\infty - T_f)\, dx}$$

$$= \frac{(2.3625 \text{ lb/hr})\ (1.01 \text{ BTU/lb} - {}^\circ\text{F})\ (293^\circ\text{F} - 229^\circ\text{F})}{(2)\ (3.1416)\ (.0848 \text{ ft})\ (39.08^\circ\text{F} - \text{ft})}$$

$$= 7.3 \text{ BTU/hr} - \text{ft}^2 - {}^\circ\text{F} \qquad \text{(with brass end plugs)}$$

*Spacing between thermocouples

EXPERIMENTAL RESULTS AND DISCUSSION

Runs 1 through 4 (each consisting of a heating period and a production period, as discussed earlier) were made in depleting the core from a volumetric liquid saturation of 100% to 0%. Experimental data for the thermodynamic paths of production for each run (for tap No. 6 in the middle of the core length) is shown in Fig. 24, relative to the vapor pressure curve for a planar interface.[1,2,3] The data is tabulated in Appendix D.

As expected from theoretical considerations, a lowering of the vapor pressure curve does occur at liquid saturations below the "irreducible" level of immiscible displacement. Each succeeding run, with a lower liquid saturation, exhibits a lower path of production. The degree of lowering is clearly beyond the range of sensing error.

The liquid saturation for each run was calculated from the steam quality obtained through a volumetric balance on the two-phase zone (see Appendix E). These values represent only an overall average for the entire two-phase zone. Gravity segregation could account for some vertical saturation gradient within the core. In addition, some error might be expected from evaporation tosses from the collection beaker, loss of uncertain amounts of water when checking pressure gauge calibrations in between runs, and uncertainty concerning the amount of water in the production Zincs between the shut-off valves and the core.

Fig. 24

EXPERIMENTAL DATA - VAPOR PRESSURE LOWERING
PRESSURE VS. TEMPERATURE FOR THE TWO-PHASE ZONE

(K = 80 md, ϕ = 0.18)

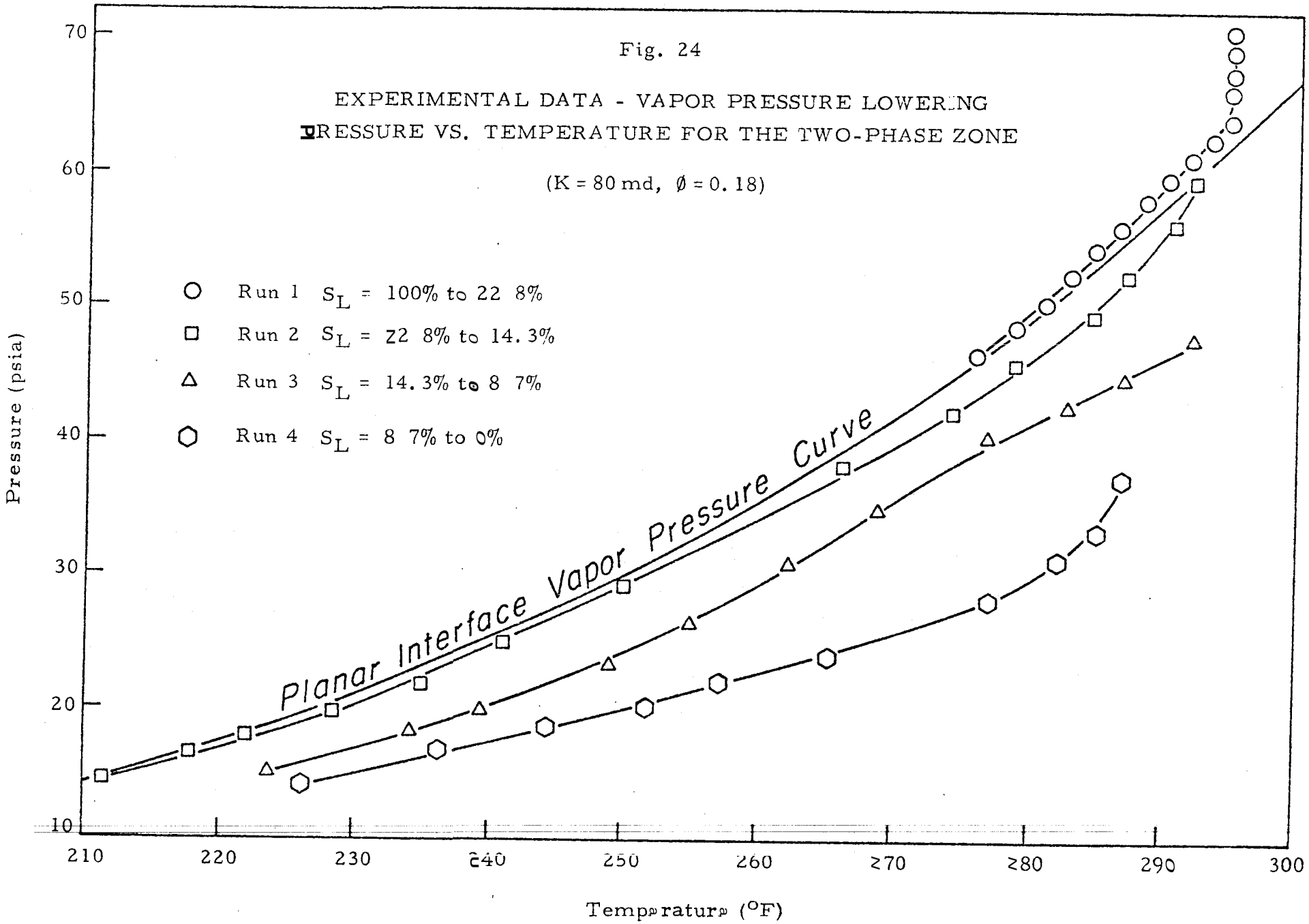

This set of experimental runs was accomplished with a negligible loss of confining pressure over a two-day period. Previous problems in this regard were solved when it was discovered that the small brass fittings which sealed off the nitrogen confining pressure from the pressure taps were too long. With these fittings bottoming out into the core, the top o-seals were compressed between the small brass fittings and the o-seal straight thread connectors above (with the expansion of the Viton sleeve upon heating) until they finally shredded, causing a nitrogen leak into the core. The fact that some taps Leaked more often was due solely to the thicker core diameter at that location. This variation in core diameter, nearly imperceptible at a glance, was the determining factor. Th problem was solved by shortening all of the small brass fittings so that they didn't bottom out. The physical model is now functioning properly without serious problems. Further data should be obtained with relative ease.

CONCLUSION

These initial experimental runs indicate that vapor pressure lowering due to interfacial tension effects does exist to a significant degree in consolidated sandstones at high temperatures. Such a phenomena, with its drastic implications toward the production forecasting and numerical simulation of geothermal reservoirs, must be studied more extensively. Future investigations should involve repeated experiments over a wide range of rock permeabilities and porosities at higher temperature levels than those at which this study was conducted. This work will be able to utilize the capacitance probe currently being developed within this project for an accurate determination of the local levels of liquid saturation at which the effect is significant.

The physical model designed and constructed in conjunction with this study provides a unique opportunity to examine the production characteristics of geothermal reservoirs--in both a physical and a chemical sense. Such work is of great importance toward a better understanding of this readily available source of energy.

REFERENCES

1. Keenan, J. H. and Keyes, F. G. : Thermodynamic Properties of Steam, John Wiley and Sons, Inc. (1936).

2. Keenan, J. H. and Keyes, F. G. : Thermodynamic Properties of Steam, John Wiley and Sons, Inc. (1967).

3. Meyer, C. A., McClintock, R. B., Silvestri, G. J. , and Spencer, R. C., Jr. : ASME Steam Tables, American Society of Mechanical Engineers, New York (1967).

4. Leverett, M. C. : "Capillary Behavior in Porous Solids," Trans. AIME (1941), 142, 152 - 169.

5. Moore, W. J. : Physical Chemistry, 3rd edition, Prentice Hall, Inc. (1962).

6. Pockells, F. : "Kapillarität," Handbuch der Physik (ed. , Winkelmann, A.), Verlag Von Johann Ambrosius Barth, Leipzig (1908), 1119 - 1160.

7. Dullien, F. A. L. and Batra, V. K.: "Determination of the Structure of Porous Media," Flow Through Porous Media, American Chemical Society, Washington D. C. (1970), 1 - 31.

8. Calhoun, J. C., Jr., Lewis, M., Jr., and Newman, R. C.: "Experiments on the Capillary Properties of Porous Solids," Trans. AIME (1949), 186, 189 - 196.

9. Ramey, H. J., Jr., Professor, Dept. of Pet. Engr., Stanford University, Personal Communication.

10. Cady, G. V. : "Model Studies of Geothermal Fluid Production," Ph. D. Dissertation, Stanford University (Nov. 1969).

11. Edlefsen, N. E. and Anderson, A. B. C. : "Thermodynamics of Soil Moisture," Hilgardia, Calif. Agric. Exp. Station, Univ. of Calif. at Berkeley (Feb. 1943), 15, No. 2, 31.

12. Poston, S. W., Ysrael, S., Hossain, A. K. M. S., Montgomery, E. F. III, and Ramey, H. J., Jr.: "The Effect of Temperature on the Irreducible Water Saturation and Relative Permeability of Unconsolidated Sands," Soc. Pet. Engr. J. (June 1970), 171-180.

13. Sinnokrot, A. A., Ramey, H. J., Jr., and Marsden, S. S., Jr.: "Effect of Temperature Level Upon Capillary Pressure Curves," Soc. Pet. Engr. J. (March 1971), 13-29.

14. Bilhartz, H. L., Jr.: "Fluid Production from Geothermal Steam Reservoirs," Master's Report, Stanford University (1971).

15. Smith, W. O.: "Mechanism of Gravity Drainage and its Relation to the Specific Yield of Uniform Sands," U. S. Geol. Surv. Prof. Paper 402-A (1961).

16. Melrose, J. C. and Brandner, C. F.: "Role of Capillary Forces in Determining Microscopic Displacement Efficiency for Oil Recovery by Waterflooding," 25th Annual Meeting of Petroleum Society of CIM, Calgary (May 1974).

17. Sanyal, S. K., Marsden, S. S., Jr., and Ramey, H. J., Jr.: "The Effect of Temperature on Electrical Resistivity of Porous Media," SPWLA 13th Annual Logging Symposium (May 1972).

18. Strobel, C. J.: "Model Studies of Geothermal Fluids Production from Consolidated Porous Media," Engineer's Thesis, Stanford University (July 1973).

19. Arihara, N.: "A Study of Non-isothermal Single and Two-phase Flow through Consolidated Sandstones," Ph. D. Dissertation, Stanford University (Nov. 1974).

20. Whiting, R. L. and Ramey, H. J., Jr.: "Application of Material and Energy Balances to Geothermal Steam Production," J. Pet. Tech. (July 1969), 893.

21. Spivak, A.: "Gravity Segregation in Two-Phase Displacement Processes," Soc. Pet. Engr. J. (Dec. 1974), 619-632.

22. Martin, J. C.: "Reservoir Analysis for Pressure Maintenance Operations Based on Complete Segregation of Mobile Fluids," Trans. AIME (1958), 213, 220-227.

23. White, D. E., Muffler, L. J. P., and Truesdell, A. H.: "Vapor-Dominated Hydrothermal Systems Compared with Hot-Water Systems," Econ. Geol. (1971), 66, No. 1, 75-97.

24. White, D. E. : "Characteristics of Geothermal Resources," Geothermal Energy (ed., Kruger, P. and Otte, C.), Stanford University Press (1973), 69 - 94.

25. Ramey, H. J., Jr., Kruger, P., and Raghavan, R. : "Explosive Stimulation of Hydrothermal Reservoirs," Geothermal Engergy (ed., Kruger, P. and Otte, C.), Stanford university Press (1973), 231 - 249.

26. Craig, H. : "The Isotopic Geochemistry of Water and Carbon in Geothermal Areas," Nuclear Geology on Geothermal Areas (ed., Tongiorgi, E.), Consiglio Naz. delle Ricerche, Rome (1963), 17 - 53.

27. Ellis, A. J. and Mahon, W. A. J. : "Natural Hydrothermal Systems and Experimental Hot-Water/Rock Interactions," Geochim. Cosmochim. Acta (1964), 28, 1323.

28. Ellis, A. J. and Mahon, W. A. J. : "Natural Hydrothermal Systems and Experimental Hot-Water/Rock Interactions (Pt. 11)," Geochim. Cosmochim. Acta (1967), 31, 519.

29. Haas, J. L., Jr. : "The Effect of Salinity on the Maximum Thermal Gradient of a Hydrothermal System at Hydrostatic Pressure," Econ. Geol. (1971), 66, No. 6, 940 - 946.

30. Lindsay, W. T., Jr. and Liu, C. T.: "Vapor Pressure Lowering of Aqueous Solutions at Elevated Temperatures," Devel. and Prog. Rpt. 347, U. S. Office of Saline Waters, Washington D. C. (1965).

31. Fournier, R. O. and Rowe, J. J.: "Estimation of Underground Temperatures from the Silica Contents of Water from Hot Springs and Wet-Steam Wells," Amer. J. Sci. (Nov. 1966).

32. Morey, G. W., Fournier, R. O., and Rowe, J. J.: "The Solubility of Quartz in Water in the Temperature Interval from 25° to 300°C," Geochim. Cosmochim. Acta (1962), 26, No. 10, 1029 - 1043.

33. Taylor, C. Research Associate, School of Earth Sciences, Stanford University.

34. Krauskopf, K. : "The Possible Role of Volatile Metal Compounds in Ore Genesis," Econ. Geol. (1964), 59, 22.

35. Facca, G. and Tonani, F. : "The Self-sealing Geothermal Field," Bull. Vulc. (1967), 27, 271.

36 Gelati, R., Ferrara, G. , and Pauichi, C. : "Evolution of Boron Content of the Steam in Larderello Geothermal Field," Second United Nations Symposium on the Development and Use of Geothermal Resources, San Francisco (May 1975).

37 Finlayson, J. B. and Mahon, W. J.: "The Chemistry of the Broadlands Geothermal Area, New Zealand," Amer. J. Sci. (Jan. 1972), 272, 38 - 68.

38. Ellis, A. J. : "Interpretation of Gas Analyses from the Wairakei Hydrothermal Area," N. Z. J. Sci. (Dec. 1962), 5, No. 4, 434 - 452.

39. Mahon, W. A. J. : "The Carbon Dioxide and Hydrogen Sulfide Content of Steam from Drillholes at Wairakei, New Zealand," N. Z. J. Sci. (March 1962), 5, No. 1, 85-98.

40. Truesdell, A. H. and White, D. E. : "Production of Superheated Steam from Vapor-Dominated Geothermal Reservoirs," Geothermics, in press.

APPENDIX A

DERIVATION OF THE EQUATION RELATING VAPOR PRESSURE TO CAPILLARY PRESSURE

(from Calhoun, Lewis, and Newman, Ref. 8)

The capillary pressure, p_c, at any height within the system is defined as:

$$p_c = p_v - p_l \qquad \text{(A-1)}$$

where

p_v is the pressure in the vapor phase (psi)
p_l is the pressure in the liquid phase (psi)

It is important to consider that both the water phase and its vapor are continuous phases within the system and that, at any point, the two phases are in equilibrium.

The gradients in the liquid and vapor columns within the porous system are:

$$dp_l = \rho_l g \, dh \qquad \text{(A-2)}$$

$$dp_v = \rho_v g \, dh \qquad \text{(A-3)}$$

where

ρ_l and ρ_v are the densities of the liquid and vapor phases, respectively (lb/ft^3)
g is gravity (ft/sec^2)
h is the height within the system (ft)

By integrating these gradients from h = o (the height at which p_c = o) to the height, h, we can evaluate p_l and p_v at height h. Note that when

$p_c = o$, $p_l = p_v$ and $p_v = p_{vo}$, the equilibrium vapor pressure above a flat interface.

For p_l, eqn. **A-2** becomes

$$\int_{p_{vo}}^{p_l} dp_l = \rho_l g \int_o^h dh \qquad (A-4)$$

As $\rho 1$ is independent of height, we find that

$$p_l = \rho_l g h + p_{vo} \qquad (A-5)$$

However, for the vapor phase, we must consider the relationship:

$$p_v = p_v M/RT \qquad (A-6)$$

where

M is the molecular weight (lb/lb - mole)
R is the ideal gas constant (10.73 psi - ft^3) (lb - mol$ - ^oR)
T is the temperature (^oR)

Thus, for p_v, eqn. **A-3** becomes:

$$\int_{p_{vo}}^{p_v} dp_v = p_v M/RT \; g \int_o^h dh \qquad (A-7)$$

or

$$\int_{p_{vo}}^{p_v} dp_v/p_v = M/RT \; g \int_o^n dh \qquad (A-8)$$

By integrating eqn. A-8, we get

$$\ln p_v/p_{vo} = Mgh/RT \qquad (A-9)$$

By combining eqns. **A-5** and **A-9**, the expressions for p_l and p_v, respectively, we can eliminate the height term h and obtain:

$$p_l = RT \rho_l/M \quad \ln p_v/p_{vo} + p_{vo} \qquad (A-10)$$

Substituting $p_l = p_v - p_c$

and $p_v = \rho_v RT/M$

into eqn. **A-10**, we get:

$$p_c - \rho_v RT/M - RT \rho_l/M \quad \ln p_v/p_{vo} - p_{vo} \qquad (A-11)$$

$$= RT\ \rho_v/M\,[1 - \rho_l/\rho_v \ln p_v/p_{vo}] - p_{vo}$$

AS

$$1 - \rho_l/\rho_v \ln p_v/p_{vo} \approx - \rho_l/\rho_v \ln p_v/p_{vo}$$

or

$$1 - \rho_l/\rho_v \ln p_v/p_{vo} \approx \rho_l/\rho_v \ln p_{vo}/p_v$$

and

$$RT\ \rho_l/M \ln p_{vo}/p_v >> p_{vo}$$

we can approximate eqn. A-11 by:

$$p_c = RT/M\ \rho_l \ln p_{vo}/p_v \qquad \text{(A-12)}$$

This equation relates p_v, the vapor pressure above a curved interface, to p_c, the capillary pressure across that interface, in terms of the measurable quantities, T, M, and ρ_l.

APPENDIX B

CALCULATION OF THE MAGNITUDE OF VAPOR PRESSURE LOWERING TO BE EXPECTED AT HIGHER TEMPERATURES

Given:

$$p_c = \sigma (1/r_1 \text{ t } 1/r_2) \qquad \text{(B-1)}$$

and

$$p_c = RT\ \rho_l/M \ln p_{vo}/p_v \qquad \text{(B-2)}$$

combining eqns. B-1 and B-2, we get:

$$\ln p_{vo}/p_v = M/\rho_l RT \quad \sigma (1/r_1 \text{ t } 1/r_2)$$

or

$$p_{vo}/p_v = \exp[M/\rho_l RT \quad \sigma (1/r_1 + 1/r_2)] \qquad \text{(B-3)}$$

The values of the constants:

M, the molecular weight of water = 18.015 lb/lb - mole

and

R, the ideal gas constant = 10.73 psi - ft3/lb - mole - ^{o}R

can be inserted into eqn. B-3 resulting in:

$$p_{vo}/p_v = \exp[1.68\sigma/\rho_l T \quad (1/r_1 \text{ t } 1/r_2)] \qquad \text{(B-4)}$$

The temperature-dependent variables are:

T, temperature in ^{o}R (^{o}F t 460^{o})

σ, interfacial tension in lb/in
(dynes/cm x 2.248 x 10^{-6} lb/dyne x 2.54cm/in)

ρ_l, density of the liquid phase (in equilibrium with the vapor phase) in lb/ft3

Interfacial tension values *were* obtained from Truesdell and White, 40

Liquid density values were obtained from saturation data from the steam tables.[2]

$T(^{o}F)$	97	250	300	350
$T(^{o}R)$	557	710	760	810
$v_l(ft^3/lb)$	0.0161	0.0170	0.0174	0.0 180
$\rho_l(lb/ft^3)$	62.03	58.82	57.31	55.59
σ(dynes/cm)	70	54	49	44
$\sigma(10^{-4}lb/in)$	3.99'7	3.083	2. 798	2.512

at $97^{o}F$

$$(1/r_1 + 1/r_2) = \rho_l RT/\sigma M \ln p_{vo}/p_v \quad (B\text{-}5)$$

$$= 5.1486 \times 10^{7} \ln p_{vo}/p_v$$

and, as

$$p_{vo}/p_v = \exp[M\sigma/\rho_l RT\ (1/r_1 + r_2)]$$

at $250^{o}F$

$$p_{vo}/p_v = \exp[1.240 \times 10^{-8}\ (1/r_1\ t\ 1/r_2)] \quad (B\text{-}6)$$

at $300^{o}F$

$$p_{vo}/p_v - \exp[1.079 \times 10^{-8}\ (1/r_1 + 1/r_2)] \quad (B\text{-}7)$$

at $350^{o}F$

$$p_{vo}/p_v = \exp[0.9380 \times 10^{-8}\ (1/r_1\ t\ 1/r_2) \quad (B\text{-}8)$$

At this point, we can now calculate the magnitude of vapor pressure lowering, p_{vo}/p_v, at the different temperature levels. From the data of Calhoun, et al., we can substitute, for each value of liquid saturation, the corresponding p_{vo}/p_v into eqn. B-5 and calculate the value for

$(1/r_1 + 1/r_2)$. Subsequently, this value of $(1/r_1 + 1/r_2)$ can be substituted into equations B-6, B-7, and B-8 in order to calculate p_{vo}/p_v for 250°F, 300°F, and 350°F, respectively. Thus, the temperature adjustment is accomplished. The results are tabulated in Table B1.

Table B1

CALCULATION OF RATIO OF FLAT SURFACE VAPOR PRESSURE TO VAPOR PRESSURE WITHIN POROUS MEDIA AT SEVERAL TEMPERATURES AND LIQUID SATURATIONS FOR CONSOLIDATED SANDSTONES

S_w	p_{vo}/p_v at 97°F	$(1/r_1+1/r_2)$ x 10^8	p_{vo}/p_v at 250°F	p_{vo}/p_v at 300°F	p_{vo}/p_v at 350°F
0.103	1.101	0.04954	1.063	1.055	1.0475
0.079	3.344	0.6215	2.161	1.955	1.790
0.069	4.796	0.8072	2.720	2.388	2.130
0.058	7.692	1.050	3.677	3.105	2.675
0.0536	9.709	1.170	4.266	3.533	2.993
0.0479	19.157	1.520	6.583	5.153	4.154
0.0382	28.903	1.732	8.559	6.475	5.066
0.0325	37.313	1.863	10.074	7.462	5.730

Fig. B1

Interfacial Tension
Between Steam and Liquid Water
As a Function *of* Temperature

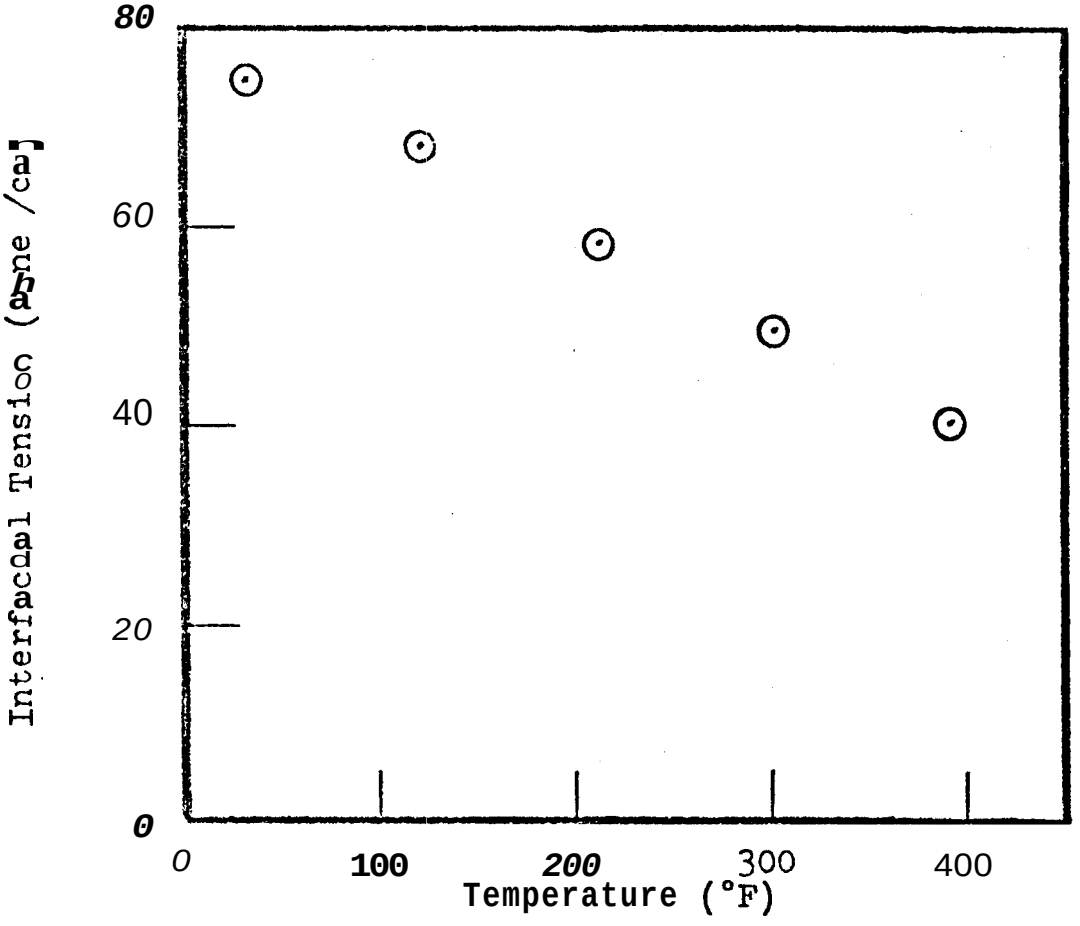

APPENDIX C

EQUIPMENT SPECIFICATIONS AND LIST OF MANUFACTURERS/SUPPLIES

Pressure Transducers

Series 6000, linear integrated circuit sensing element
100 mv = 300 psi
Combined error (linearity t hysteresis): ± .5% full scale

Perry Wallia, Monolithic Transducers, Inc.
1954-Q Old Middlefield Way
Mountain View, California 94040
(415) 967-0953

Pump

Controlled volume diaphragm pump
Maximum rate: 2.8 gal/hr
Model R111A

Milton Roy Company
1243 Alpine Road, Suite 108
Walnut Creek, California 94598
(415) 937-6771

Mass Balance

Ohaus Triple Beam Balance
Capacity: 2610 gin
Accuracy: 0.1 gm

c/o **Peninsula** Scientific
2185 Park Boulevard
Palo Alto, California 94306
(415) 326-4136

Thermocouples

Xactpak assembly
Iron-constantan
Accuracy: ± 2°F
Grounded junction
Transition fitting

Claud S. Gordon Co.
916 American Street
San Carlos, California
(415) 591-7070

Temperature Recorder

Speedomax W model
12-point sweep recorder
Range: 0 - 500°F

Leeds and Northrup Co.
700 S. El Caniino Real
San Mateo, California
(415) 349-6656

Pressure Gauee

Ashcroft Duragauge
Range: 0 - 100 psig
Precision reading to one-half psi
316 SS tube and socket

c/o N. J. Hatter and Co.
330 Hatch Drive
Foster City, California
(415) 574-1300

Air Bath

Blue M mechanical convection oven
Floor model POM - 1406C - 1
Temperature range: to 650°F
Inside dimensions: 48" (w) x 24" (d) x 36" (h)

Blue M Electric Company
Blue Island, Illinois

c/o Van Water and Rogers
3745 Bayshore Boulevard
Brisbane, California
(415) 369-5561

Pressure Recorder

Chessel flatbed recorder
Single pen with low thermal effects switch
17 ranges from 0.5mV to 100V
Zero suppression capability of 1, 2, or 3 times the range in use
Continuously adjustable zero from -50 to +150 scale divisions
Event marker option

c/o Nick Humeny Instruments
P. O. Box 634
Belmont, California 94002
(415) 593-8392

Pressure Repulator

Model 2 - 580 (for nitrogen)

Matheson Gas Products
6775 Central Avenue
Newark, California
(415) 793-2559

Viton Sleeve

70 duro Viton sleeve
2.062" ID x 0.250" wall x 26" Long
Smooth surface

West American Rubber Co.
750 N. Main Street
Orange, California 92668
(714) 532-3355

Natural Core

Berea sandstone
2" diameter
Permeability: 100md
Porosity: 18%

Cleveland Quarries Co.
Amherst, Ohio 44001
(216) 986-4501

Modular Power Supply Units (for transducers)

Model MMS/O - .120
Output voltage: 10V
Output current: 120mA

Sorensen Company
676 Island Pond Road
Manchester, New Hampshire 03103

c/o Instrurnent Specialists, Inc.
2359 De La Cruz Boulevard
Santa Clara, California
(408) 244-1505

Swagelok Tube Fittings, Whitey, and Nupro Valves

Van Dyke Valve and Fitting Co.
1240 Eirchwood Drive
Sunnyvale, California
(408) 734-3145

Tubing

Tubesales
1730 Geary Boulevard
San Francisco, California
(415) 361-1919

Viton 0-Rings

Parker o-seals

c/o McDowell and Company
26203 Production Avenue, Building 2
Hayward, California
(415) 785-7744

Carbide Drillbits (No. 51)

Kobb-Jack Corp.
1130 Independence Avenue
Mountain View, California
(415) 961-3100

APPENDIX D

Table D1

RUN 1 - PRODUCTION

Time (min.)	Temperature (^{o}F) and Pressure (psia)											Cumulative Production (gm)
	T_1	P_2	T_3	T_4	T_5	P_6	T_7	T_8	T_9	P_{10}	T_{11}	
0	296	92.1	294	293	294	92.1	295	296	297	92.1	297	0
15	296	79.0	295	294	294	78.5	295	296	296	76.3	297	4.0
30	296	74.6	296	295	295	74.1	296	296	297	71.2	297	11.1
45	296	72.0	296	295	295	71.6	296	296	296	68.8	296	17.8
60	296	70.3	296	295	295	69.8	296	296	296	66.6	294	24.1
75	296	69.6	296	295	295	69.2	296	296	296	68.0	296	27.0
90	297	70.9	296	296	296	70.5	297	297	297	69.7	297	27.3
105	297	71.9	296	296	296	71.7	296	296	297	70.9	297	27.3
120	297	69.8	296	296	296	68.8	296	296	295	64.3	292	30.8
135	296	67.6	295	295	295	66.8	295	294	293	62.0	288	35.0
150	296	66.6	296	295	295	65.5	295	294	293	60.7	289	38.9
165	296	65.9	295	295	295	64.6	295	294	293	60.6	289	41.8
180	296	65.6	295	295	294	64.5	294	293	293	60.8	290	43.9
195	296	64.7	295	295	294	63.5	295	292	291	57.8	287	48.1
210	295	64.2	294	294	293	62.6	292	291	289	56.7	287	51.3
225	295	63.6	294	294	293	61.9	292	291	289	55.8	288	54.4
240	294	63.0	293	293	292	61.3	291	289	287	54.6	288	57.6
255	293	62.4	292	291	291	60.1	289	287	286	53.6	289	61.2

Table D.I (cont.)

RUN 1 - PRODUCTION

Time (min.)	Temperature (°F) and Pressure (psia)											Cumulative Production (gm)
	T_1	P_2	T_3	T_4	T_5	P_6	T_7	T_8	T_9	P_{10}	T_{11}	
270	293	62.4	292	292	291	59.3	288	287	285	52.7	289	65.1
285	293	61.7	291	291	290	58.4	287	286	283	52.4	290	68.3
300	292	61.4	291	290	289	57.9	287	286	284	51.8	291	72.2
315	292	61.1	291	290	288	57.0	286	283	280	49.1	291	76.8
330	292	60.1	290	289	287	55.6	284	281	278	47.6	291	82.3
345	292	59.5	289	288	287	54.6	283	280	277	46.9	292	87.5
360	292	59.0	289	288	286	54.0	282	280	277	46.4	293	92.8
375	291	58.1	288	286	284	52.6	280	278	275	44.1	293	99.7
390	290	57.0	287	285	283	51.6	278	277	274	43.1	293	105.9
405	290	55.6	286	284	282	50.6	277	276	277	41.8	294	112.7
420	289	54.5	284	282	281	49.6	271	275	280	41.1	293	120.0
440	290	52.8	283	282	280	48	277	276	285	39.8	294	128.5
451	290	51.8	281	279	278	47.8	276	277	286	38.8	294	132.9
465	291	50.9	280	279	277	47 1	276	282	288	30.1	295	138.2
480	291	49.9	279	278	276	46 1	277	285	290	36.7	295	144.9

Note: 15 gm lost fr both P_6 and P_{10} in calibration ck between runs.

Table D2

RUN 2 - PRODUCTION

Time (min.)	Temperature (^{o}F) and Pressure (psia)											Cumulative Production (gm)
	T_1	P_2	T_3	T_4	T_5	P_6	T_7	T_8	T_9	P_{10}	T_{11}	
0	293	63.6	292	292	292	63.6	292	293	294	63.6	294	0
15	292	59.6	292	292	292	59.2	293	293	293	58.8	293	3.95
30	289	56.1	289	289	290	55.9	292	292	293	55.9	291	4.3
45	286	51.7	286	286	286	51.9	289	289	289	52.0	287	5.1
60	278	48.7	282	282	282	49.0	284	284	283	48.4	280	6.4
75	272	44.6	278	279	279	45.6	277	280	279	43.5	274	8.5
90	264	41.6	271	273	272	41.6	272	273	271	38.1	266	10.1
105	257	37.9	265	267	266	37.7	265	266	265	32.5	260	12.1
120	249	34.5	256	260	257	34.5	255	257	256	26.6	253	13.8
135	242	30.8	250	253	251	28.6	247	251	252	23.4	247	15.3
150	234	28.0	242	245	242	24.3	240	243	244	20.8	240	16.5
165	226	25.6	235	238	236	21.8	234	236	238	19.4	234	17.0
180	220	23.6	227	232	230	19.6	227	230	232	19.4	227	17.2
195	212	21.6	221	224	223	17.7	221	223	225	17.5	221	17.2
210	206	20.1	215	219	218	16.6	217	218	220	16.6	216	17.2
225	200	18.9	208	212	212	14.6	210	211	212	14.6	209	17.2

Table D3

RUN 3 - HEATUP

Time (min.)	Temperature (°F) and Pressure (psia)										
	T_1	P_2	T_3	T_4	T_5	P_6	T_7	T_8	T_9	P_{10}	T_{11}
0	203	17.7	204	204	205	14.7	203	204	207	14.7	216
15	236	17.7	217	216	216	17.4	216	219	224	17.4	256
30	258	18.7	236	233	233	21.9	236	241	245	21.9	277
45	269	20.5	246	248	248	26.9	252	256	261	26.0	286
60	275	24.4	250	255	257	29.7	262	267	272	29.7	289
75	282	30.5	257	263	267	32.9	264	277	282	33.6	292
90	284	32.5	260	267	272	34.2	278	282	284	34.7	293
105	286	36.2	265	272	276	37.0	282	285	287	37.5	293
120	287	39.5	269	276	281	39.7	286	288	290	40.4	294
135	289	42.3	272	279	283	42.5	288	289	291	42.8	294
150	288	44.7	274	281	284	44.7	288	290	291	44.8	292
165	290	46.6	280	284	287	46.7	291	292	293	46.7	295
180	291	47.7	284	286	288	47.7	291	292	292	47.7	294

Table D4

RUN 3 - PRODUCTION

Time (min.)	Temperature (^{o}F) and Pressure (psia)											Cumulative Production (gm)
	T_1	P_2	T_3	T_4	T_5	P_6	T_7	T_8	T_9	P_{10}	T_{11}	
0	293	51.2	292	292	292	51.2	293	294	294	51.2	295	0
15	292	47.3	291	291	291	47.2	293	294	294	47.2	294	1.9
30	288	45.7	289	289	290	45.7	292	292	291	44.9	290	2.8
45	284	44.1	286	287	287	44.5	287	288	288	43.9	286	4.1
60	277	42.7	282	283	283	42.2	283	283	282	39.7	279	5.7
75	270	40.3	276	278	277	40.2	277	278	278	36.4	275	6.4
95	259	38.9	267	270	269	34.5	267	269	269	31.4	265	8.4
107	253	34.7	262	265	263	30.4	261	263	265	27.7	260	9.3
120	245	31.8	254	257	256	26.4	254	256	257	24.0	252	10.2
135	238	28.8	246	251	250	22.8	248	250	251	20.5	247	10.9
158	226	25.2	234	239	241	19.2	238	238	241	18.0	236	11.2
170	221	24.0	228	234	236	17.9	233	234	235	17.5	231	11.5
195	210	19.9	217	223	225	14.7	222	223	224	14.7	220	11.5

Table D5

RUN 4 - HEATUP

Temperature (^{o}F) and Pressure (psia)

Time (min.)	T_1	P_2	T_3	T_4	T_5	P_6	T_7	T_8	T_9	P_{10}	T_{11}
0	206	19.7	214	220	221	14.7	218	219	221	14.7	195
60	225	19.0	232	230	231	18.9	231	233	237	18.6	266
78	265	20.2	246	246	246	21.9	250	252	257	23.8	282
97	276	23.4	252	258	260	25.2	266	268	272	26.7	291
109	280	25.2	257	265	267	27.5	273	276	279	28.2	283
120	283	27.3	260	269	272	29.5	277	280	283	29.8	294
140	287	29.7	268	276	278	31.0	284	286	288	31.7	295

Table D6

RUN 4 - PRODUCTION

Time (min.)	Temperature (°F) and Pressure (psia)											Cumulative Production (gm)
	T_1	P_2	T_3	T_4	T_5	P_6	T_7	T_8	T_9	P_{10}	T_{11}	
0	291	51.9	292	293	292	46.9	292	293	292	38.4	292	4.0
15	285	46.8	287	290	287	37.2	287	290	290	31.2	289	7.7
30	280	42.5	283	287	285	32.9	286	287	288	27.5	286	9.8
45	272	39.2	276	282	282	30.7	282	283	284	25.5	281	11.6
60	264	36.2	270	277	277	27.7	277	278	279	23.2	265	13.8
75	249	30.5	257	264	266	23.5	265	265	266	20.1	262	16.0
105	241	28.1	250	256	258	21.7	257	258	259	18.8	255	16.8
120	235	22.7	244	251	252	19.9	251	252	253	17.8	249	17.9
135	227	19.9	237	243	245	18.2	244	244	245	16.9	241	18.0
150	220	17.4	230	236	237	16.5	236	237	238	16.5	233	18.1
165	210	14.6	221	225	227	14.6	225	225	227	14.6	221	18.1

APPENDIX E

CALCIJLATION OF LIQUID SATURATION IN THE CORE

Development of the Equations

A volumetric balance is used to obtain an expression for the steam quality within the core.

$$v_p = [v_l (1 - X) \ \mathbf{t} \ v_s X] w_t \qquad \text{(E-1)}$$

where

v_p is the pore volume of two-phase zone (ft^3)
v_l is the specific volume of liquid water (ft^3/lb)
v_s is the specific volume of saturated steam (ft^3/lb)
w_t is the total fluid mass (lb)
X is the fraction of the total fluid mass which is steam

Solving eqn. E-1 for X, we get:

$$X = \frac{v_p/w - v_l}{v_s - v_l} \qquad \text{(E-2)}$$

This calculated value of X from eqn. E-2 gives us the ratio:

$$X = w_s / w_s + w_l = w_s/w_t \qquad \text{(E-3)}$$

where

w_s is the weight of steam (lb)
w_l is the weight of liquid water (lb)

This gives us one equation and two unknowns. We can use the conservation of mass for the second equation.

$$w_t = w_s \ \mathbf{t} \ w_l = w_{ti} - w_{tp} \qquad \textbf{(E-4)}$$

where

w_{ti} is the initial fluid mass (lb)
w_{tp} is the mass of produced fluid (lb)

Thus, we can calculate w_s and $w_{1'}$

Knowing w_s and $w_{1'}$ we can calculate S_L, the average volumetric liquid saturation for the two-phase zone:

$$S_L = w_l v_l / w_l v_l + w_s v_s \qquad \text{(E-5)}$$

Pertinent Information

Expected pore volume = ϕv

$= \phi \pi r^2 1$

$= (0.182)\ (3.1416)\ (1.009\ \text{in})^2\ (23.188\ \text{in})$

$= 13.378\ \text{in}^3$

$= 219\ \text{cm}^3$ (cc)

Actual mass produced:

144.9 gm	Run 1
29.3	lost in calibration check
17.2	Run 2
11.5	Run 3
18.1	Run 4
221.0 gm	

The above seem to check (1gm/cc at room temperature).

Calculations

Given: $v_p = 221\ \text{cc} = 0.0078045\ \text{ft}^3$

$w_i = 221\ \text{g} = 0.4872\ \text{lb}$

v_l (294°F) = 0.01739 ft^3/lb

vs (294°F) = 7.048 ft^3/lb

Run 1: initial average S_L = 100%

Run 2: $$X = \frac{1.0078045\ ft3\ /\ (221\ g\ -\ 174.2\ g)\ (1\ lb/453.6\ g)] \ -\ 0.01739\ ft^3/lb}{7.048\ ft^3/lb\ -\ 0.01739\ ft^3/lb}$$

= 0.829%

.00829 = w_s/w_t = w_s/. 103175 lb

w_s = 0.000855 lb

$w_l = w_t - w_s$ = .103175 lb - .000855 lb = .10232 lb

Initial average S_L = $$\frac{(.\ 10232\ lb)\ (.01739\ ft^3/lb)}{(.\ 10232\ lb)\ (.01739\ ft^3/lb)\ t\ (.000855\ lb)\ (7.048\ ft^3/lb)}$$

= 22.79%

Run 3: $$X = \frac{[.0078045 ft^3/(221\ g\ -\ 191.4\ g)\ (1lb/453.6\ g)] \ -\ 0.01739 ft^3/lb}{7.048\ ft^3/lb\ -\ 0.01739\ ft3/lb}$$

= 1.45%

.01454 = w_s/w_t = w_s/.06526

w_s = 0.0009488 lb

$w_l = w_t - w_s$ = .06526 lb - .0009488 lb = 0.06431 lb

Initial average S_L = $$\frac{(.\ 06431\ lb)\ (.\ 01739\ ft^3/lb)}{(.06431\ lb)\ (.01739\ ft^3/lb)\ t\ (.0009488\ lb)\ (7.048\ ft^3/lb)}$$

= 14.34%

Run 4: $$X = \frac{[.0078045\ ft3/(221\ g - 202.9\ g)\ (1\ lb/453.6\ g)] - .01739\ ft3/lb}{7.048\ ft^3/lb - .01739\ ft^3/lb}$$

$$= 2.5370$$

$$.02535 = w_s/w_t = w_s/.03990$$

$$w_s = .00101\ lb$$

$$w_l = w_t - w_s = .03990\ lb - .00101\ lb = .03889\ lb$$

Initial average $$S_L = \frac{(.03889\ lb)\ (.01739\ ft^3/lb)}{(.03889\ lb)\ (.01739\ ft^3/lb) + (.00101\ lb)\ (7.048\ ft^3/lb)}$$

$$= 8.7\%$$

Table E 1

AVERAGE LIQUID SATURAT ON FOR TWO-HASE ZONE

Run	Initial Fluid Mass (gm)	Initial Liquid Saturation (294°F)	Mass Produced (gm)	Mass Remaining (gm)
1	221.7	1.000	174.9	46.8
2	46.8	0.228	17.2	29.6
3	29.6	0.143	11.5	18.1
4	18.1	0.087	18.1	0